CHAPTER 1

Introduction

1.1 Problem statement and Motivation

Most of the reservoirs worldwide are carbonate reservoirs (**Figure 1.1**). The regional distribution of 120 giant fields discovered in 2000–2012 illustrates that the highest contribution (54.5%) in global scale comes from the marine carbonate reservoirs and some (12%) from the lacustrine carbonate reservoirs (Bai and Xu, 2014). Moreover, the carbonate reservoirs accounts for 40% of the world's total hydrocarbon production (Ray, 2014). It is significantly important to apply reservoir geophysics tools to analyze carbonates for oil and gas exploration and development.

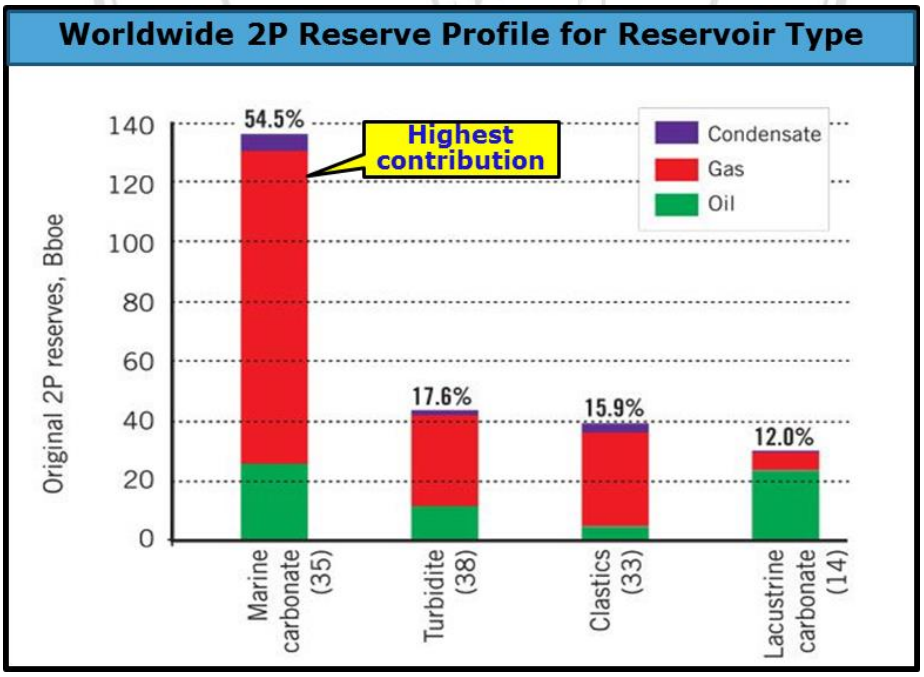

Figure 1.1. Worldwide 2P reserve profile for reservoir type distribution during 2000-2012 from 120 global giant fields (modified from Bai and Xu, 2014).

Normally, it is difficult to predict carbonate reservoir properties, reservoir facies or fluid type directly because there is no distinguishing feature such as bright spot to define and amplitude maps do not work as expected in clastic reservoirs. Unlike clastic reservoirs, carbonate reservoirs tend to have complicated pore types each of which contains different compressibilities affecting different seismic wave velocities. Besides pore types, factors that influence seismic wave velocities in carbonates include mineral, porosity, pore fluid type and saturation, and reservoir parameters such as pressure and temperature (Wang, 1997). The prediction in carbonate reservoir geometry is also difficult due to complex original depositional facies and the impact of diagenesis causing the requirement of large numbers of drilled wells in many fields of carbonate reservoirs.

Interestingly, the use of geophysical methods could provide a fundamental understanding of seismic responses to reservoir properties and their dynamic changes by exploiting seismic technology on 2D/3D seismic data. In the last 3-4 decades, there has been increased interest in the use of compressional (P)-wave velocity, shear (S)-wave velocity and density in conjunction with angle to constrain the properties of the subsurface after the approximations of Zoeppritz equations have been published by Aki and Richards (1980). Those studies are able to delineate the link between reservoir properties (e.g. fluid type, lithology) and the seismic signatures to guide reservoir characterization in an area with very sparse well control. The integration of reservoir characterization into an exploration/appraisal program should minimize the number of wells required and help to establish the reservoir geometry and/or facies.

Whitcombe et al. (2002) established the extended elastic impedance (EEI) method by introducing the use of the chi (χ) angle instead of angle of incidence for AVO analysis. They used the reference or the normalizing constants Vp_0, Vs_0, and ρ_0 (Vp= P-wave velocity, Vs =S-wave velocity and ρ=density) in the computation of elastic impedance to improve the dimensionality and units (Whitcombe, 2002). The application of extended elastic impedance (EEI) inversion is expected to provide the reservoir characterization by identifying the fluid type: water- or hydrocarbon-bearing reservoir, in the target zone by using limited well control and seismic data. The zone of interest or target zone in the current study is one carbonate reservoir of the Natih formation in

Block A, onshore Oman **(Figure 1.2)**. The main idea of this research is to integrate the seismic inversion results to improve interpretation accuracy and enhance the ability in fluid type discrimination. This can be a useful tool for prospect evaluation in exploration and/or development programs which could be used to optimize the choice of drilling locations and reduce risk and uncertainty.

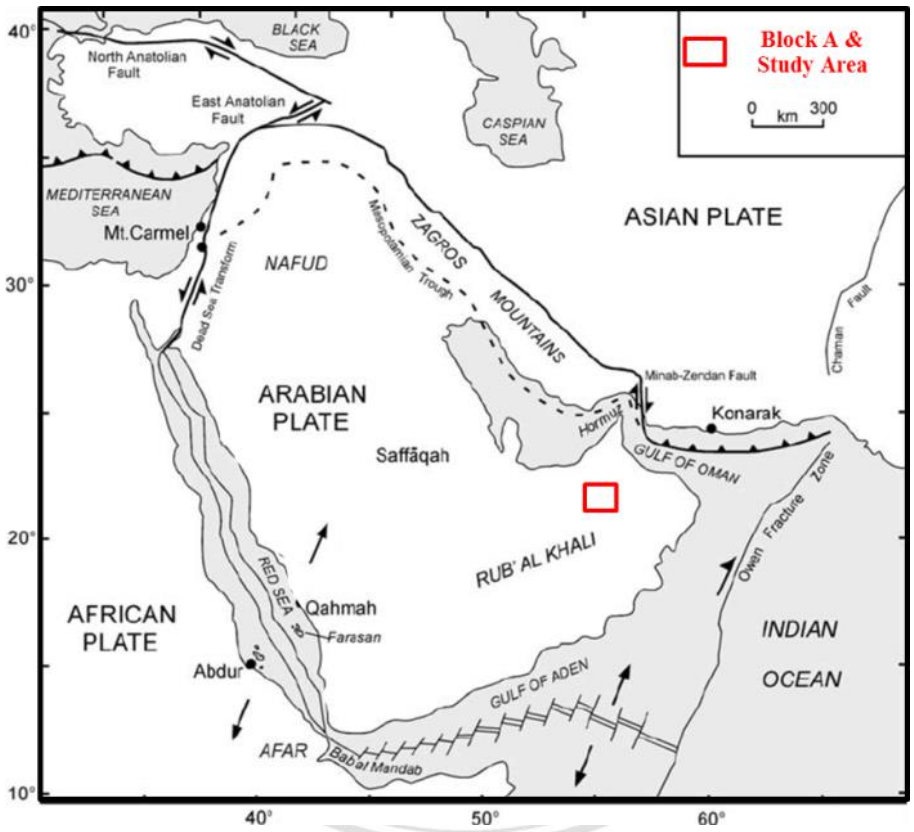

Figure 1.2. General map of the Arabian Peninsula and adjacent regions (modified from Bailey et al., 2007).

1.2 Research objectives

The objective of this research is to identify the fluid type in a carbonate reservoir of the Natih formation.

1.3 Overview of the study area

1.3.1 Geologic background

The study area **(Figure 1.3)** is the field of carbonate reservoirs in Block A, onshore Oman. Oman is situated on the southeast margin of the Arabian Plate and is close to the borders of the Asian, Indian, and African plates **(Figure 1.2)**. It is bordered by the Gulf of Aden to the south, the Owen Fracture Zone to the east, and the complex Zagros Mountains to the north. This area has undergone six tectonic episodes from Late Precambrian to Present (Pollastro, 1999) that comprised (1) continental evolution and island arc accretion, (2) and (3) intra-plate rifting, wrenching and epeirogenic tectonics, (4) continental break-up and development of a passive margin, (5) active margin tectonics involving ophiolite obduction and (6) collision in the north and salt flow creating salt traps.

The general Oman stratigraphy can be separated into four sections **(Figure 1.4).** First, the Upper Precambrian to Lower Paleozoic (I) that is comprised of two groups; Huqf and Haima, in which Huqf consists mainly of shallow marine carbonates with salts and Haima consists mainly of shallow marine clastics. Second, the Upper Paleozoic (II) comprised of Haushi and Akhdar in which there are glacial sediments and platform carbonates. Third, the Mesozoic section (III) consists of platform carbonates with some marine shales of primarily Natih and Shuaiba formations. Fourth, the Tertiary section (IV) consists mainly of platform carbonates and clastics.

The Natih Formation is one of Oman Cretaceous Petroleum Systems which were deposited in the North Oman foreland basin (Borowski, 2016). In general, it can be divided into seven litho-stratigraphic units: A – G **(Figure 1.5)**. However, in this study area, the Natih E, F and G Units are only presented by drilling evidence **(Figure 1.6)**. The Nahr Umr and Shuaiba formations are older than Natih formation. The younger Lower Fiqa formation is on top of Natih formation as shown in **Figures 1.5 - 1.6**.

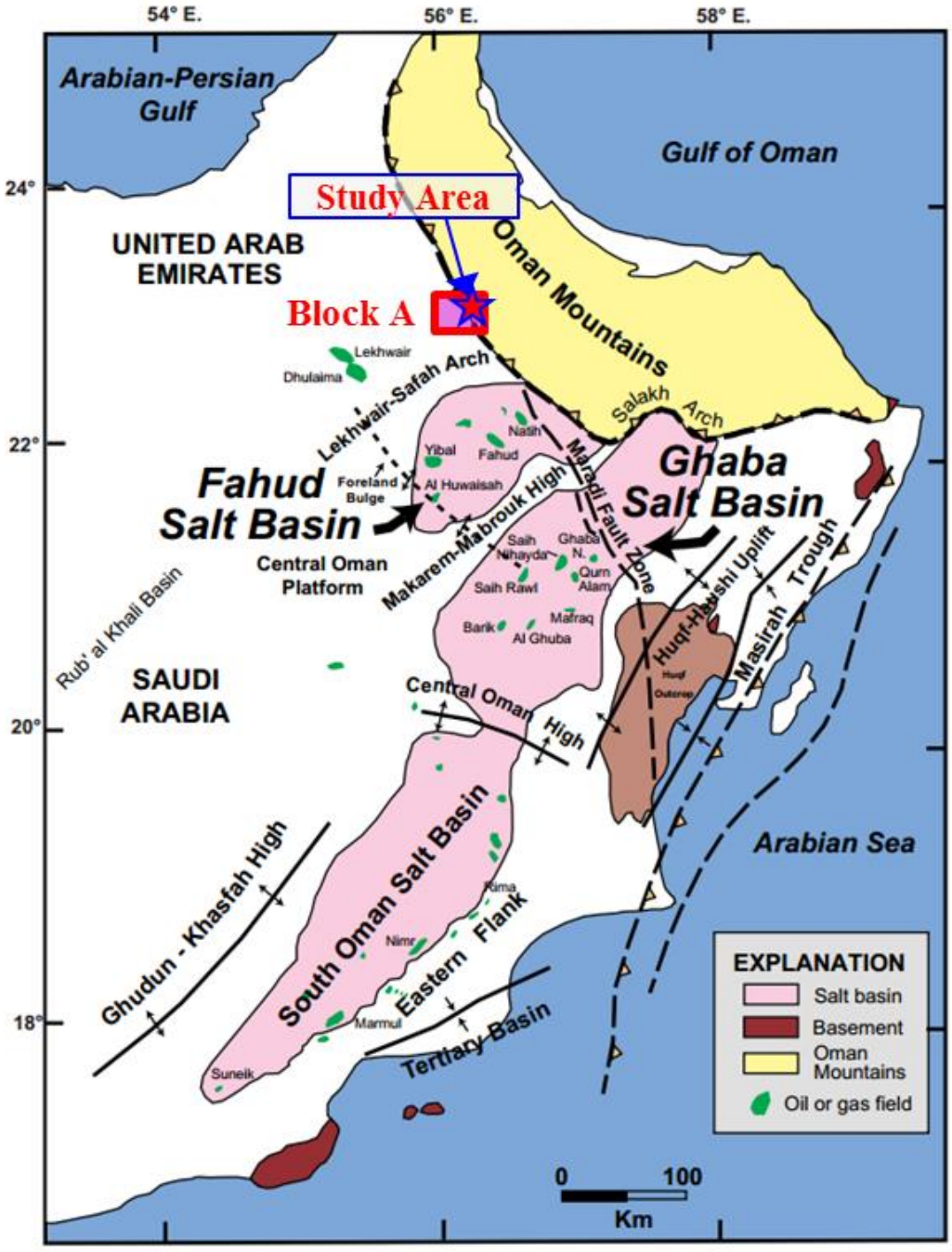

Figure 1.3. Map showing major geological elements and fields of Oman, location of Block A and study area (modified from Pollastro, 1999).

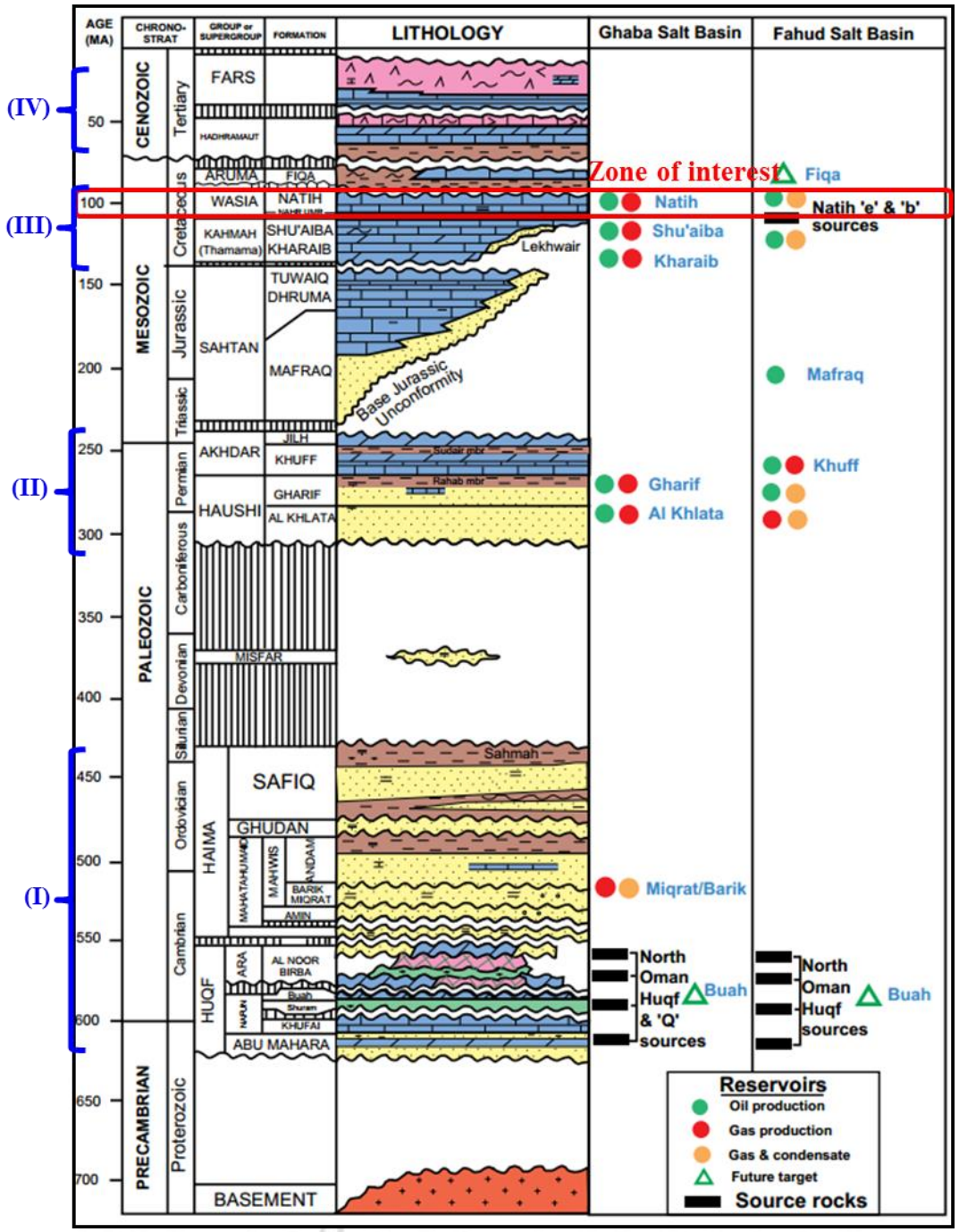

Figure 1.4. General Oman Stratigraphy (modified from Pollastro, 1999).

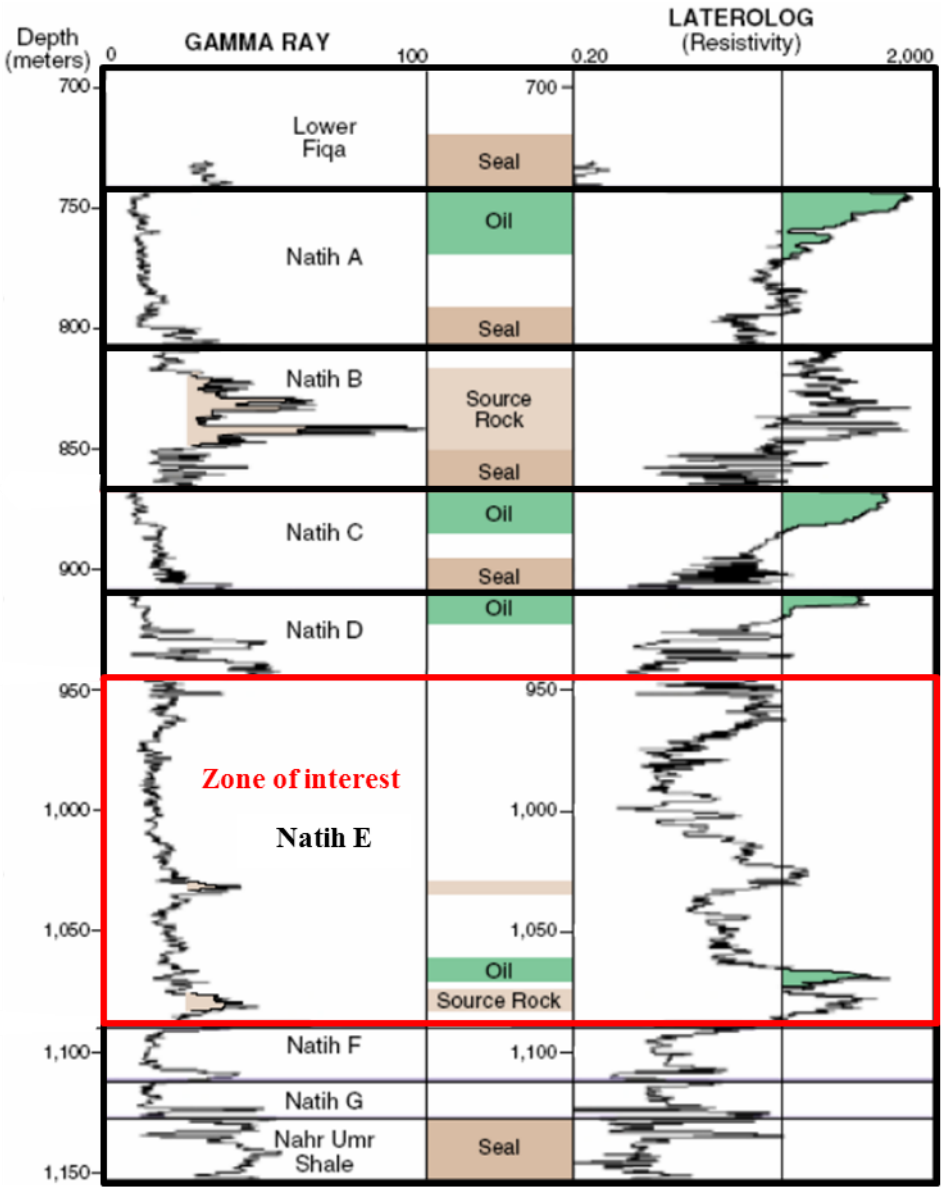

Figure 1.5. Schematic showing the Natih formation type log and seven litho-stratigraphic units from the Natih-3 well (modified from Borowski, 2016).

1.3.2 Hydrocarbon accumulations

Hydrocarbon accumulations have been recognized in carbonate and clastic units throughout the stratigraphic section of the northern part of Oman, especially in the Ghaba and Fahud Salt Basins. Most of hydrocarbon occurrence has been proven within reservoirs of Cretaceous, Carboniferous - Permian, and Cambrian-Ordovician age because of their proximity to excellent overlying seals (Pollastro, 1999). The main Cretaceous carbonate reservoirs are the Natih and Shuaiba formations **(Figures 1.4 and 1.6)** where the Fiqa formation is a shale seal for Natih and the Nahr Umr formation is a shale seal for the Shuaiba. Petroleum system and hydrocarbon occurrence can be analogously applied to this study area because they are situated in the same geological setting and petroleum province.

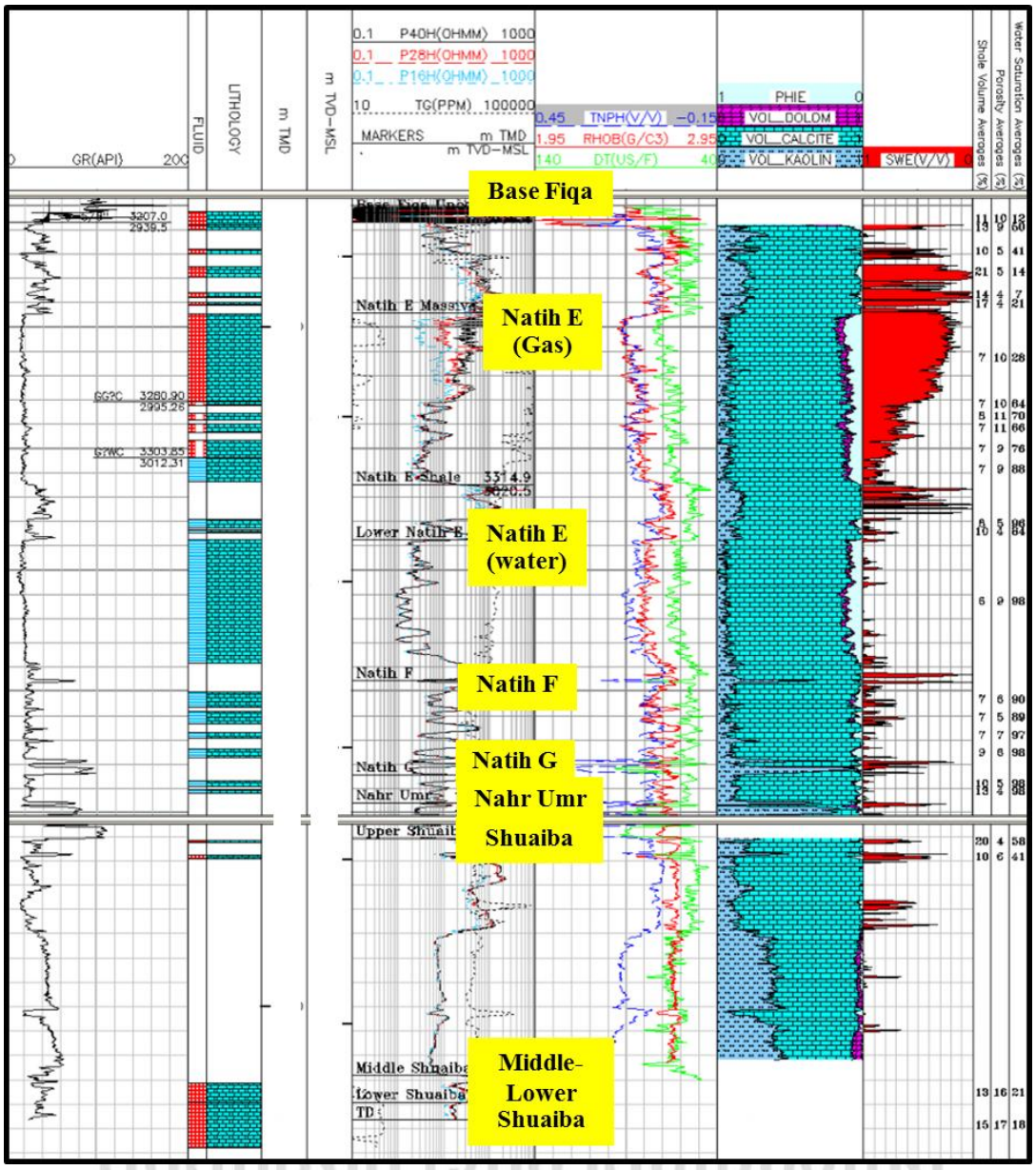

Figure 1.6. The proven hydrocarbon accumulation in the sample well.

1.4 Data inventory

1.4.1 Well Data

Well log data from four selected wells were used in this research: wells A1, A2, A4, and A8. Moreover, one well that is located outside the study (**Figure 1.7**) area, well A7, was used for establishing the S-wave empirical equation and another well would be used to do a blind well test at the end of study. The well logs, whether wireline logging (WL) or logging while drilling (LWD), were acquired in those wells as summarized in **Table 1.1**. There are gamma ray, caliper, deep resistivity, neutron porosity, density, water saturation, volume of clay, P-wave and S-wave sonic, and check shot. The quality of the WL/LWD logs will be discussed in the following. The P-wave sonic and density logs are available in all wells (A1, A2, A4, and A8), but S-wave sonic logs exist only in 2 wells (A7 and A8). However, the S-wave sonic log in well A7 covers only the upper part of Natih E interval, that is approximately 100 m thick, and this log in well A8 lacks data in some intervals (**Figure 1.8**).

To validate the S-wave sonic log, well A7 and well A8 will be quality-controlled as much as possible. Fortunately, the uniform characteristics of platform carbonates in the Natih formation should aid the S-wave sonic log correction and/or estimation by using these two well data at least to guide trending or confirming the robustness of the S-wave sonic log, as discussed in the next section. The check shot data also exist in these two wells: well A2 and A4 and others will use check shot from nearby well due to similar structure in the vicinity.

The main geological well tops (Markers) include the Base Fiqa, Top Natih E, Top Nahr Umr and Top Shuaiba, whose tops of formations were picked based on rate of penetration (ROP), cuttings description, total gas while drilling and offset well correlation.

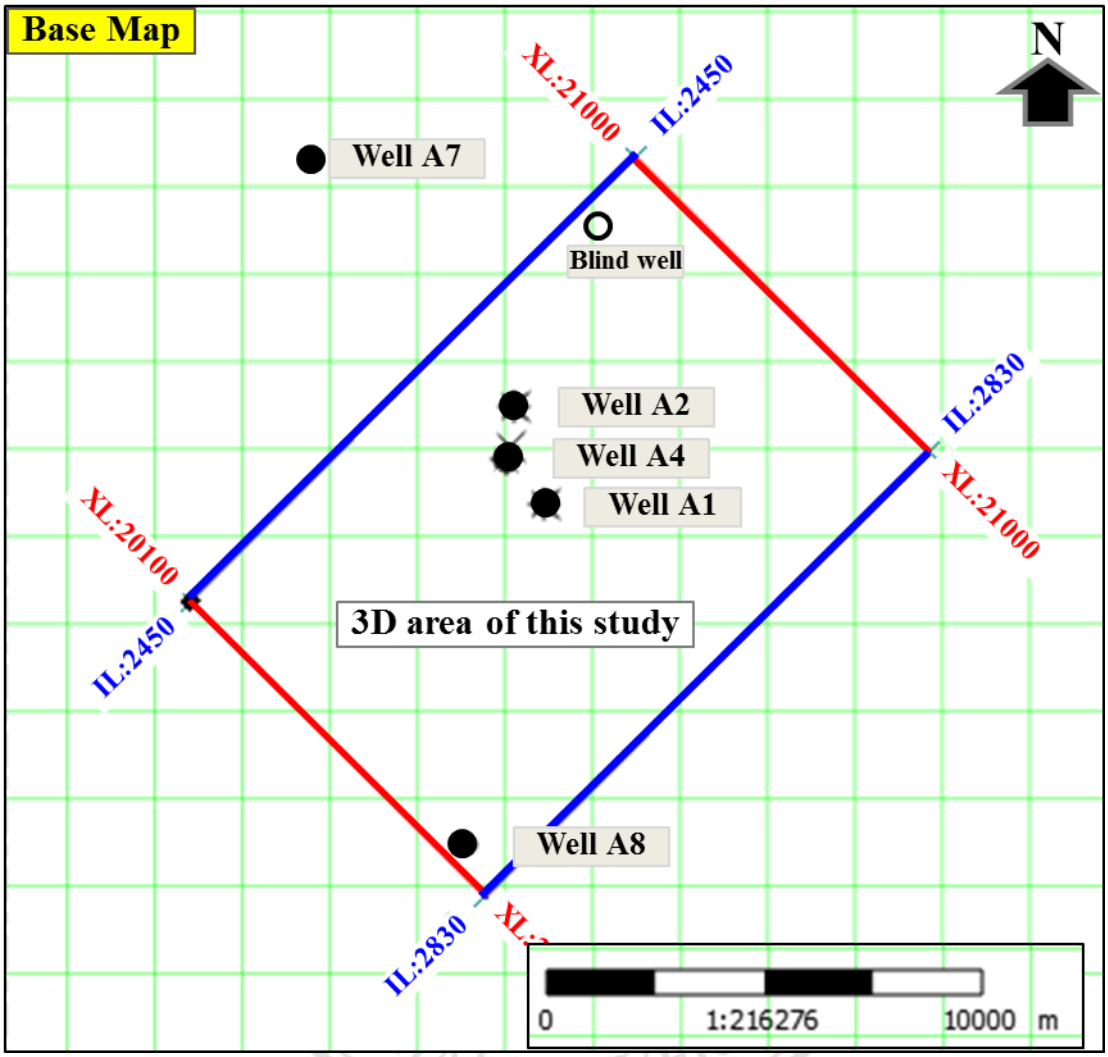

Figure 1.7. The base map shows 3D seismic area and well positions of this study. The inline direction (Blue lines) is southwest (SW) – northeast (NE) which is orthogonal to the crossline (Red lines) of northwest (NW) – southeast (SE).

Table 1.1. The summary of available well log from 4 wells (inside study area) and 1 well (well A7 is outside study area).

Well Name / Log Type	Well A1 (WL)	Well A2 (WL)	Well A4 (WL)	Well A8 (LWD)	Well A7 (LWD)
Gamma Ray (GR)	√	√	√	√	√
Caliper (CALI)	√	√			
Resistivity (LLD)	√	√	√	√	√
Neutron Porosity (NPHI)	√	√	√	√	
Density (RHOB)	√	√	√	√	
Water saturation (Sw)	√	√	√	√	
Volume of clay (VCL)	√	√	√	√	
P-wave sonic (DT)	√	√	√	√	√
S-wave sonic (DTSM)				√	√
Check shot		√	√	√	

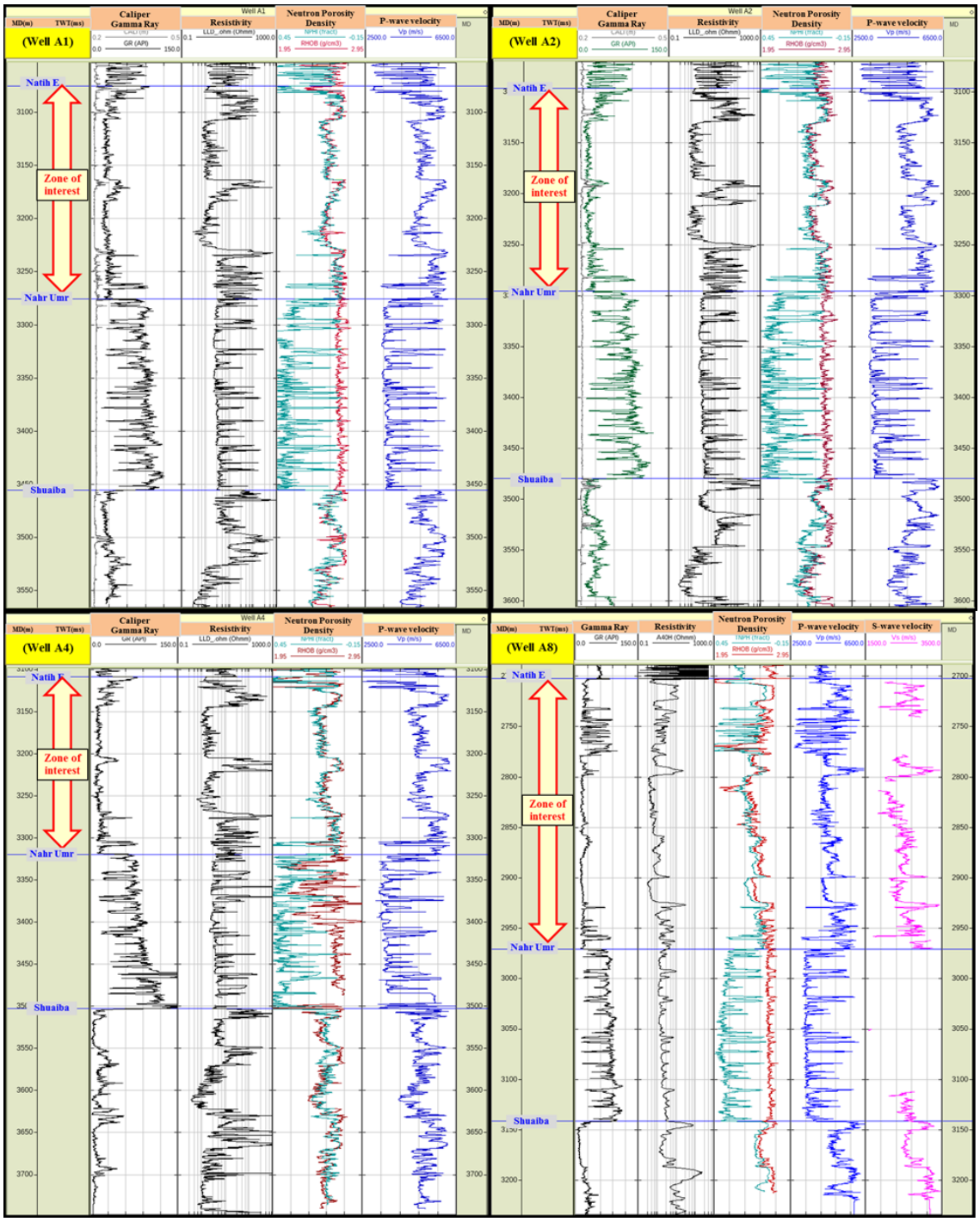

Figure 1.8. The summary well logs available in this study area including well A1 (Top left), A2 (Top right), A4 (Bottom left), and A8 (Bottom right).

1.4.2 Seismic Data

The 3D seismic data for this study are pre-stack time migrated (PSTM) gathers. The 3D survey area is covered by inline 2450 – 2830 and crossline 20100 - 21000 (**Figure 1.7**). The data are negative standard polarity which an increase of impedance (a positive reflection coefficient) corresponding to a trough (Sheriff and Geldart, 1995). On other hand, it represents "European polarity" (Brown, 2001). The other parameters are present in **Table 1.2**. The anisotropy perspective is not expected in this study because the previous study of this area stated that no significant fractures.

Table 1.2. General parameters of 3D seismic data.

Polarity	European	**Source type**	Vibroseis
Phase	Zero	**Geodetic datum**	Fahud
Record length	6 sec	**Spheroid**	Clarke 1880
Sampling interval	2 ms	**Projection type**	UTM
Bin size	12.5 m X 25 m	**Zone**	40
Source interval	50 m	**Year of survey**	1999
Group interval	25 m	**Year of reprocessing**	2013

1.4.3 Horizon Interpretation

Four key horizons were interpreted: Near Base Fiqa, Near Natih E, Near Top Nahr Umr, and Near Top Shuaiba. Horizons of Near Base Fiqa and Near Natih E were interpreted on seismic troughs (the interface between low to high acoustic impedance).

1.5 Quality control

1.5.1 Quality control of well log data

Conventionally, these well logs are the keys to a variety of geophysical and geomechanical methods, especially in reservoir characterization. In that purpose, the robustness of log measurements is necessary and critical. In this study, P-wave sonic and density logs are available in all selected 4 wells and their qualities are fair to good; hence, log conditioning is needed. In contrast, the S-wave sonic logs exist reliably only in well A7 and A8. There are some gaps of data in well A8 (**Figure 1.9**) and limited depth coverage in well A7 (**Figure 1.10**). The P-wave and S-wave sonic logs exist for only about 100 m in well A7.

1.5.1.1 P-wave and S-wave sonic logs

Those sonic logs were logged during drilling with 8.5 inches of open-hole using synthetic water-based mud and used the monopole source of acoustic log measurement. The situation with logging while drilling (LWD) is more complex because there is a large steel collar in logging tools affecting the measurement of formation S-wave slowness, that is the inverse of velocity (Tang and Cheng, 2004; Cheng, 2015). Besides that, several uncertainties in the dispersion behaviour such as mud velocity, tool centralization/mode contamination, hole size, and mud weight (density) could affect the improper acoustic measurement making some gaps of S-wave sonic data as shown in **Figure 1.9**.

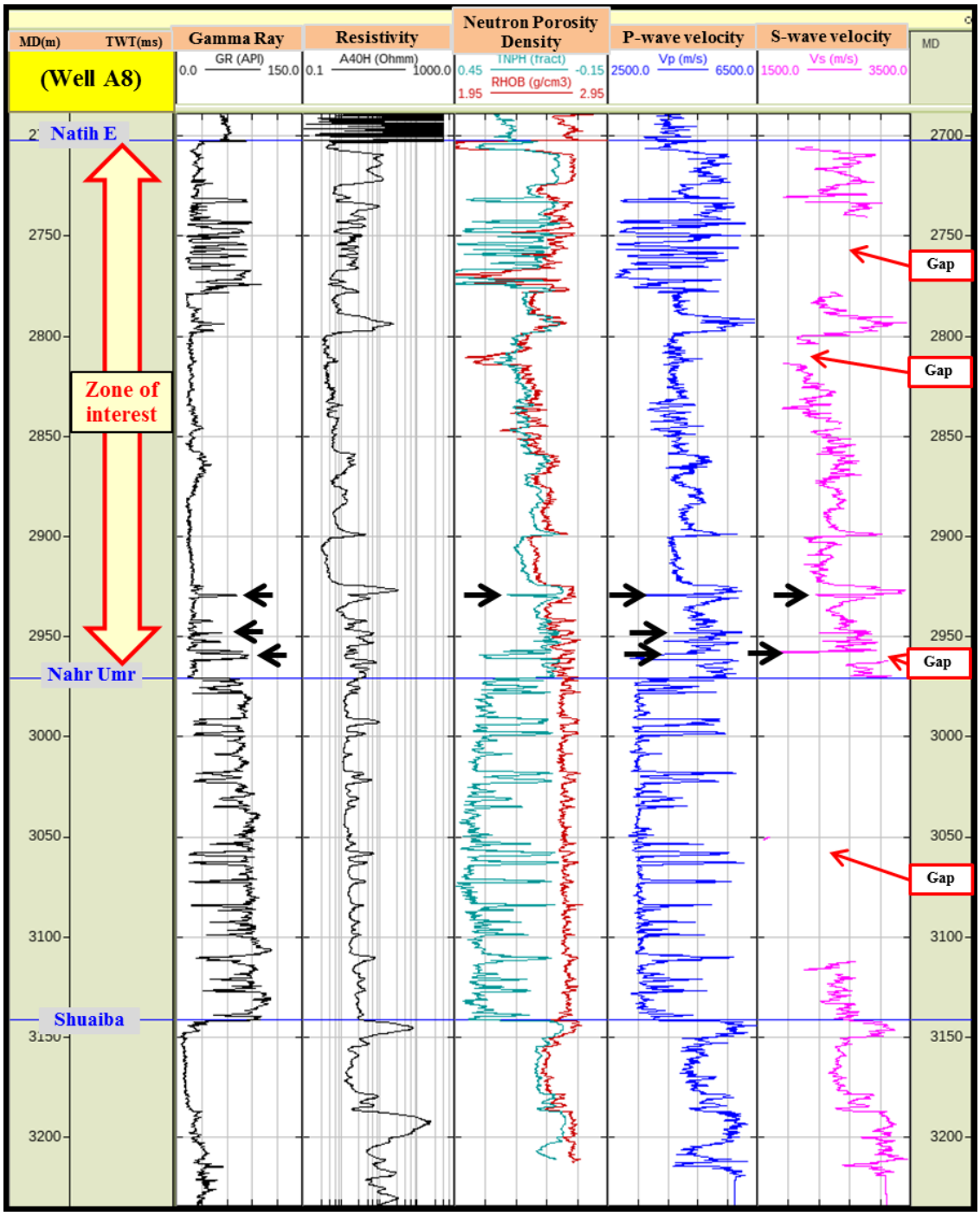

Figure 1.9. The well log overview of well A8 acquired by LWD. Some gaps (Red arrows) and spikes (Black arrows) are highlighted.

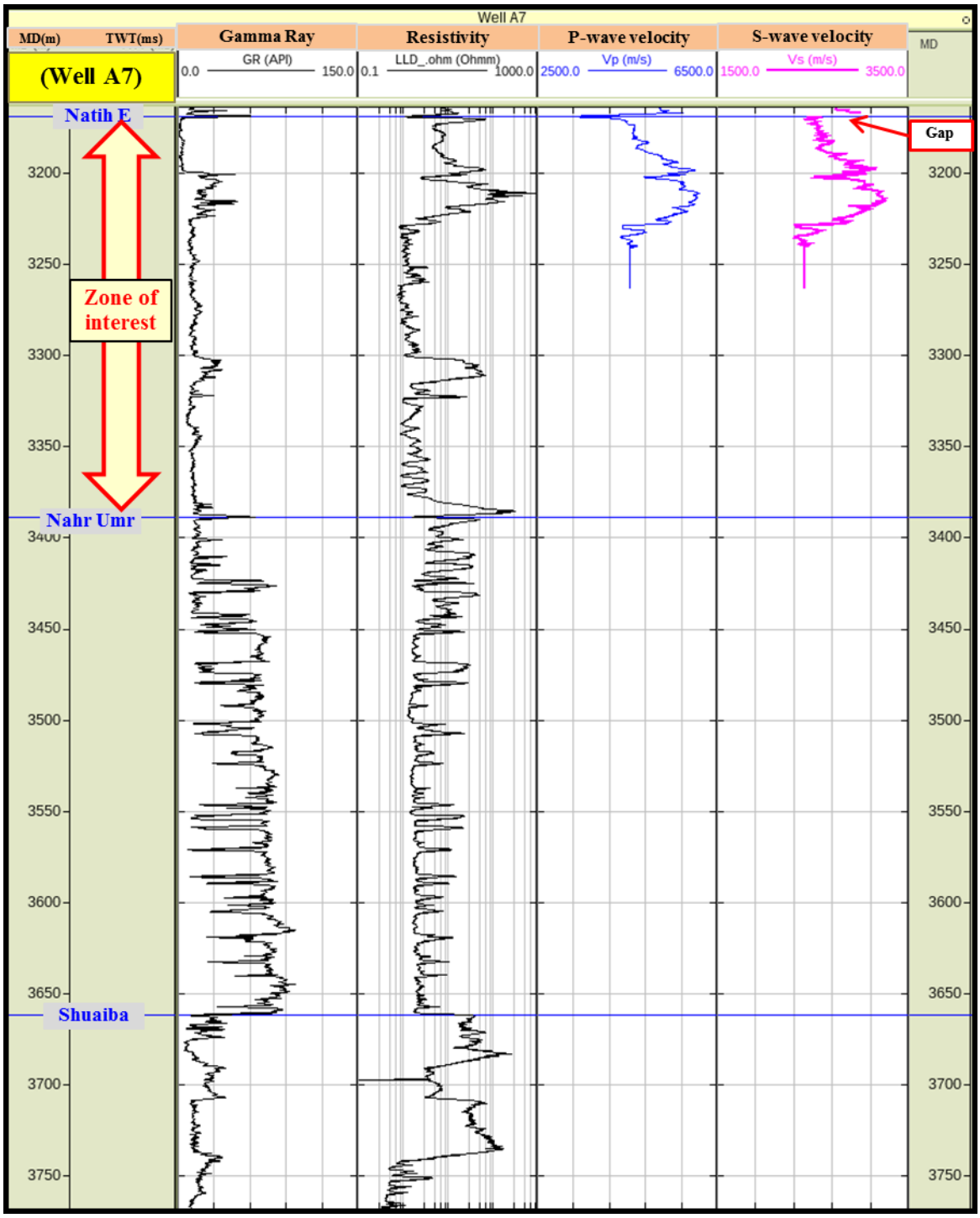

Figure 1.10 The well log overview of well A7 acquired by LWD.

To assess log quality, the P-wave and S-wave velocities (Vp and Vs) from those logs are cross-plotted at each well in which the interval of Natih E is selected (**Figure 1.11**). From the figure, Vs values of well A7 range from 2,250 to 3,250 m/s and Vs values of well A8 are in the range of 2,000 to 3250 m/s.

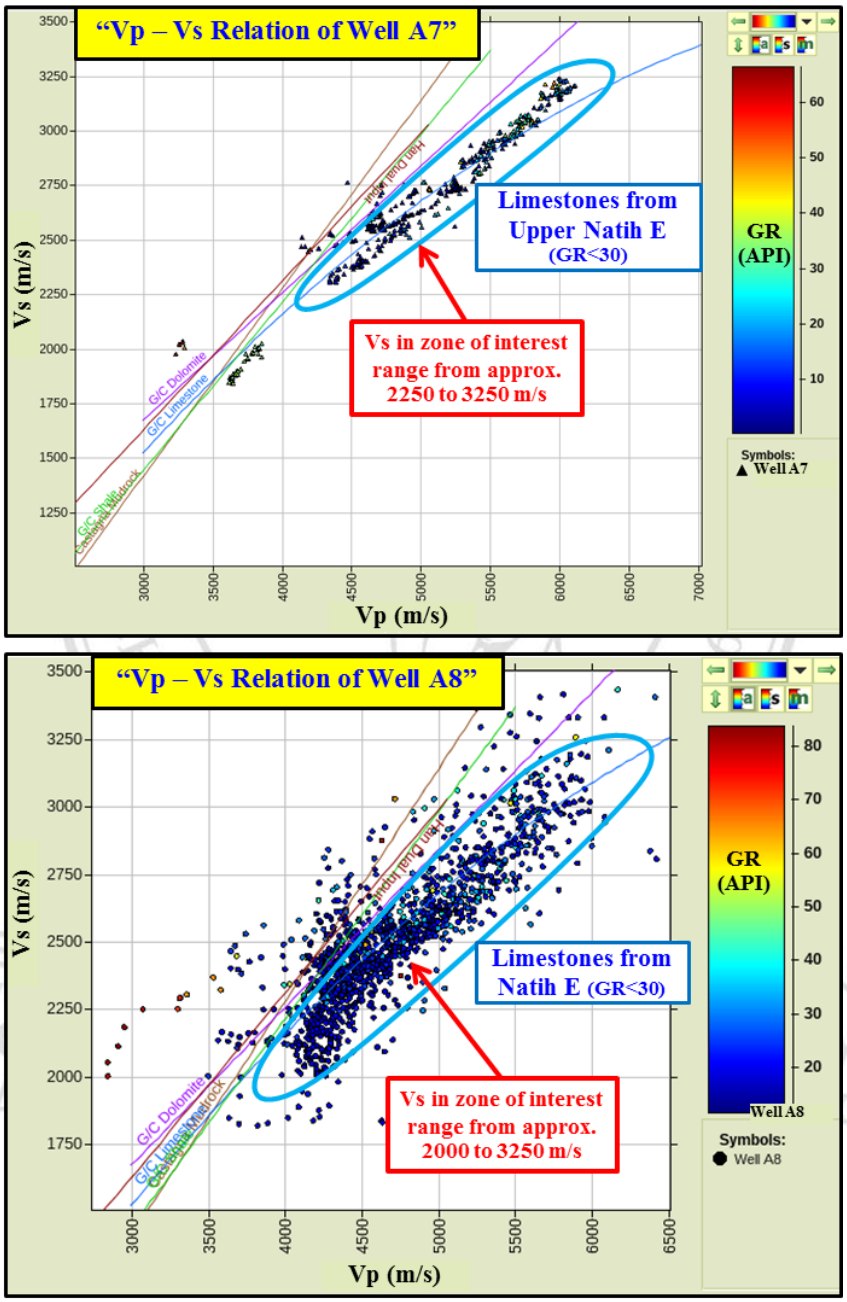

Figure 1.11. Cross-plots of P-wave and S-wave velocities (Vp and Vs) from wells A7 and A8, illustrating the Natih E interval.

Fortunately, the Vp versus Vs relation clearly shows that the points of GR less than or equal to 30 API units fall mainly near the Greenberg-Castagna (G/C) Limestone line[1], the points of GR between 50 and 70 scatter in the region of G/C shale and Castagna Mudrock[2], and the points of GR higher than 70 API lie above those lines (**Figure 1.12**). This interpretation of facies groups is limestone (Light blue oval), mudstone (Navy oval) and shale (Green oval), respectively.

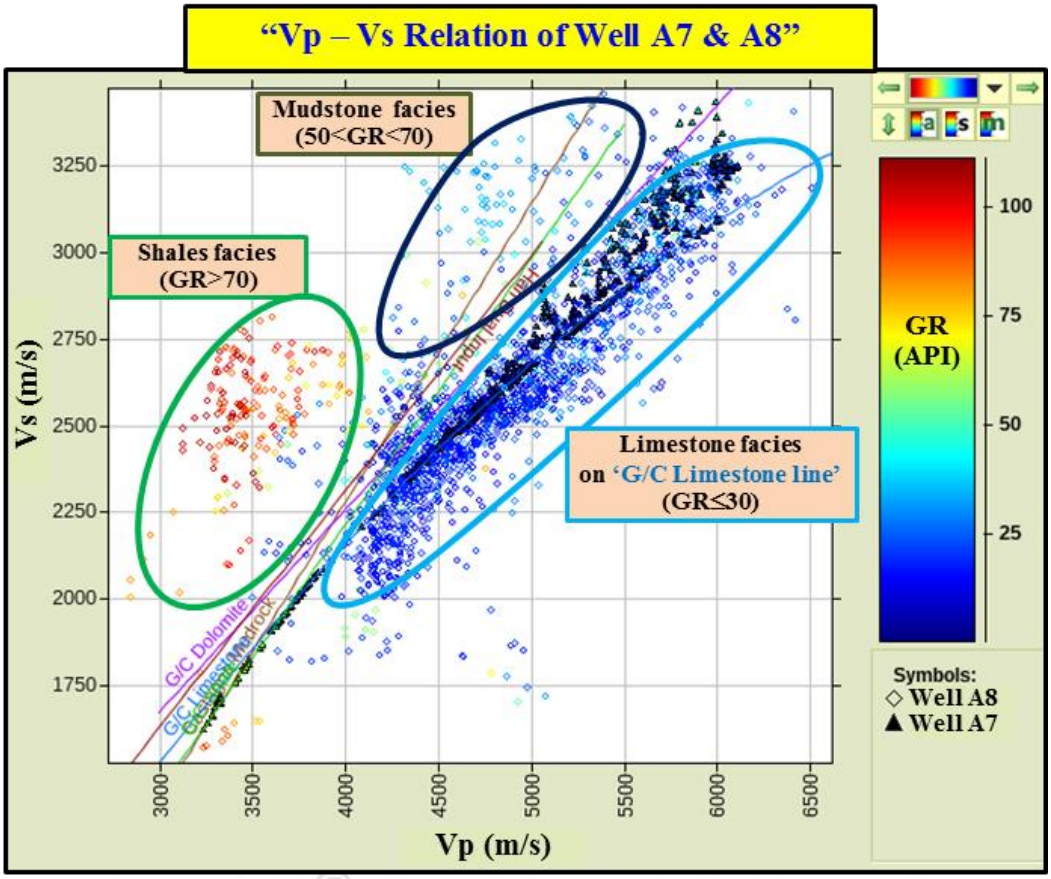

Figure 1.12. The summary plot showing the three facies groups derived from Vp-Vs relation of well A7 and A8 using whole well interval.

As shown in the above cross-plots, the robustness of P-wave and S-wave sonic logs are high, however, the gap intervals in S-wave velocity (Vs) log should be estimated by Vp to Vs relation which is obtained from available log data set (Discuss in next section).

Before going to estimation, we need to better understand the fundamentals and velocity variations in carbonate rocks. Anselmetti and Everli (1993) studied the velocity measurement in carbonates over 200 samples from different areas, ages and compaction stages. They stated that Vp and Vs in Cretaceous carbonate rocks vary from 3,000 to 6,500 m/s and from 1,700 to 3,400 m/s respectively (at 8 MPa effective pressure). These samples are Cretaceous carbonate platform facies similar in deposition and age of the Natih formation in this study. The P-wave and S-wave velocities (Vp and Vs) of dry and fully water-saturated limestone samples were investigated by Assefa et al. (2003) that they were measured at 50 MPa effective pressure, as shown in **Figure 1.13**. The range of Vp and Vs in both situations is 3,300-5,500 and 1,800-3,000 m/s, which are in conformity with former study. In Ameen et al. (2009)'s case study, the velocities of Arab-D carbonate reservoirs (Jurassic in age) located in Ghawar field, Saudi Arabia, 700 km to the west of this study area, are demonstrated as 3,400-7,000 m/s (Vp) and 1,700-4,000 m/s (Vs) (**Figure 1.14**).

Besides that, P-wave to S-wave velocity (Vp/Vs) ratios of approximately 1.82 (dolomites) and 1.95 (limestones) have also been examined in detail by Johnston and Christensen (1992). These values align with Vp/Vs ratio reported in the literature (e.g. Pickett, 1963; Castagna et al., 1985) that are 1.8 and 1.9 respectively. In 1993, Anselmetti and Everli pointed out that Vp/Vs ratio in carbonate rocks is roughly 1.9–2.0. In the meantime, Assefa et al. (2003) concluded the averages of Vp/Vs ratio for dry, oil-saturated and water-saturated limestones are 1.71±0.02, 1.84±0.01 and 1.89±0.02 respectively, for the given range of porosity (3-17%).

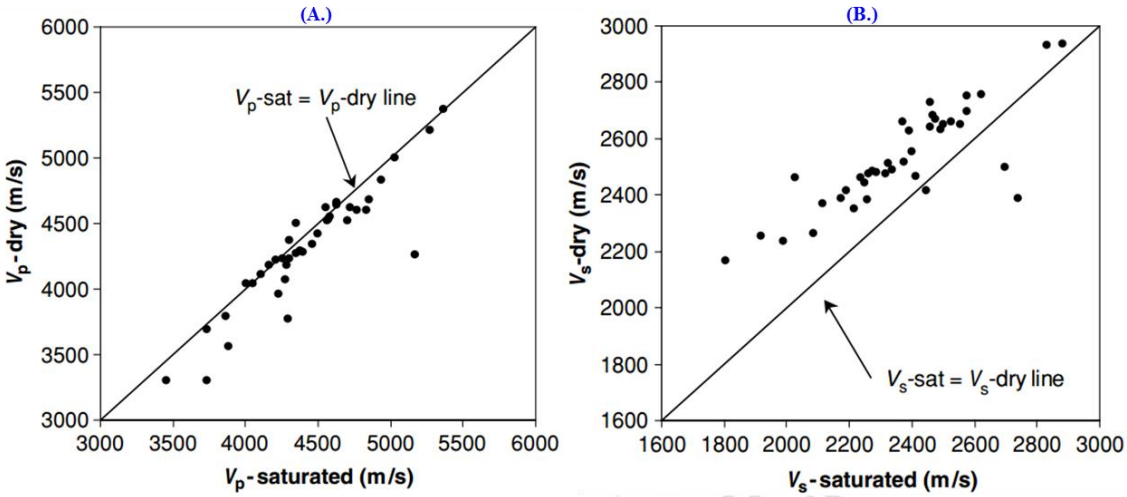

Figure 1.13. The schematic showing the Vp (A.) and Vs (B.) of dry and fully water-saturated limestone samples at 50 MPa effective pressure (modified from Assefa et al., 2003).

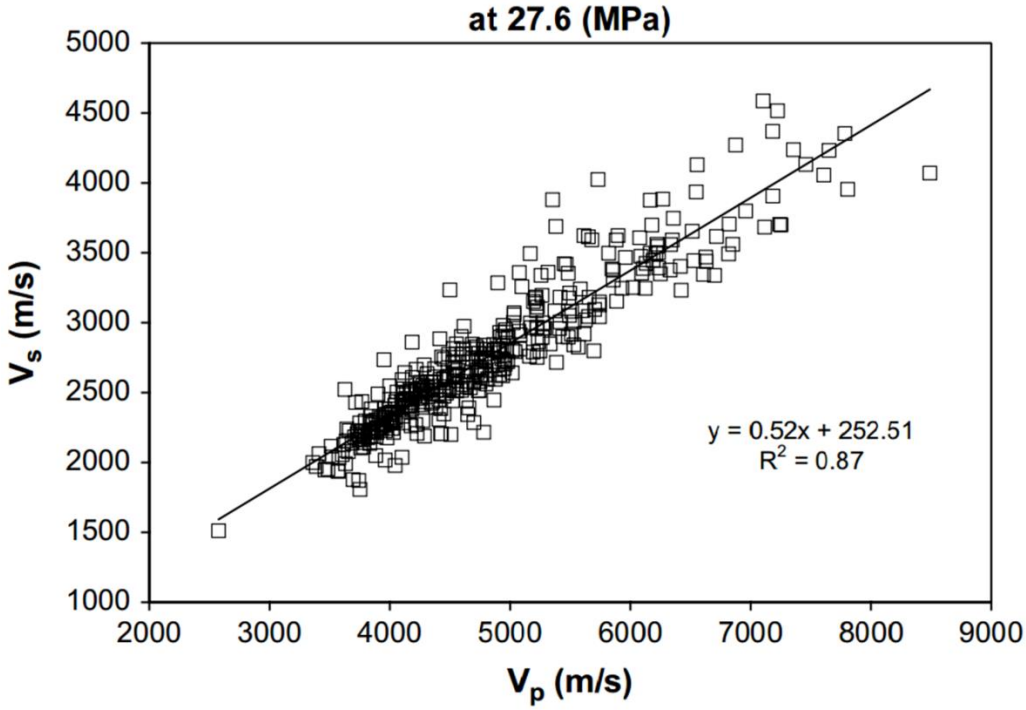

Figure 1.14. The correlation of Vp versus Vs and velocity-derived formula for Arab-D carbonate reservoir (Ameen et al., 2009).

When we lack S-wave velocity (Vs) log measurements for a comprehensive subsurface study, several methods have been proposed to estimate Vs from other available data, such as assuming Poisson's ratio (Wantland, 1964), measuring elastic properties of rocks in a laboratory (Birch, 1960; Christensen, 1974, Rafavich et al., 1984; Anselmetti and Everli,1993; Assefa et al., 2003) or using empirical correlations (Castagna et al., 1993; Brocher, 2005, 2008; Ameen et al., 2009). Laboratory measurements generally are not tied directly to seismic data, but rather are used to establish the systematics of velocity variation (Castagna et al., 1993). Continuous measurements of S-wave velocity as a function of increasing depth in a borehole are generally required for calibration of the seismic response (Castagna et al., 1993). However, the empirical correlations have been developed for a specific area and their use in other fields is subject to uncertainties. Therefore, sufficient caution and skepticism when applying any empirical manners to the Vs estimation will enable one to enhance robustness and reliability.

1.5.1.2 S-wave velocity estimation

In recent decades, many researchers have published a variety of approaches (e.g. Greenberg and Castagna, 1992; Castagna et al., 1993; Brocher, 2005), based on laboratory core analysis, well logs, and numerical modeling to predict Vs from Vp. However, most of those studies have focused on sandstones. To predict a more comprehensive empirical model for carbonates, which here is limestone, a number of models have been combined to derive one equation across them all.

In 1963, Pickett stated that Vs greater than 1,500 m/s the simple Vs equation as function of Vp for limestone can be expressed:

$$Vs = Vp/1.9 \quad \text{(Equation 1.1)}$$

where Vp and Vs are P-wave and S-wave velocities respectively.

However, at lower Vs (<1,500 m/s) Greenberg and Castagna (1992) and Castagna et al. (1993) gave representative polynomial relations for estimating Vs from Vp, depending on data derived from sonic log as below:

$$Vs = -0.05509(Vp^2) + 1.0168(Vp) - 1.0305 \quad \text{(Equation 1.22)}$$

where Vp and Vs are in km/s and for limestone.

In 2005, Brocher's compilation has been introduced at which the empirical equation of Vs as a function of Vp can be seen as below:

$$Vs = 0.7858 – 1.2344(Vp) + 0.7949(Vp^2) – 0.1238(Vp^3) + 0.0064(Vp^4) \quad \text{(Equation 1.3)}$$

where Vp and Vs are P-wave and S-wave velocities respectively and in km/s. This equation is valid for velocities range between 1.5–8.5 km/s (Brocher, 2005).

Another Vs equation obtained from Arab-D carbonate reservoir (Ameen et al., 2009) is:

$$Vs = 0.52(Vp) + 252.51 \quad \text{(Equation 1.4)}$$

In order to obtain better empirical correlation between Vp and Vs, the Vp-Vs relationships from well A7 and A8 in Block A are also established and subsequently the linear regression and its equation (Equation 5) is expressed in **Figure 1.15 (C.)**.

$$Vs = 0.5343(Vp) – 7.1039. \quad \text{(Equation 1.5)}$$

The reference pore fluid of Natih E in both wells is mostly water saturated, with 8-18% of effective porosity. The formation pressure and temperature at borehole condition collected from nearby wells ranges from 20 to 32 MPa (2900-4650 psi) and 100 to 120°C.

The five equations are compared in **Figure 1.16 (A)**. **Figure 1.16 (B)** shows the (A) plot with measured Vs values from the A7 S-wave sonic log. The reliability of Vs estimation is explicitly determined here because the points of actual Vs (measured Vs) from logs (taken from limestone and limestone with mudstone) lie near the estimated Vs using equations 1, 2 and 5 (i.e. by Pickett, 1963; Castagna et al., 1993; Phaungphuak, 2016 in prep); therefore the fit function of a second-order polynomial could be established based on the excellent agreement between actual data and estimation as:

$$Vs = -0.00004(Vp^2) + 0.9275(Vp) - 918.86 \quad \text{(Equation 1.6)}$$

where Vp and Vs are in m/s and the correlation coefficient is 0.97.

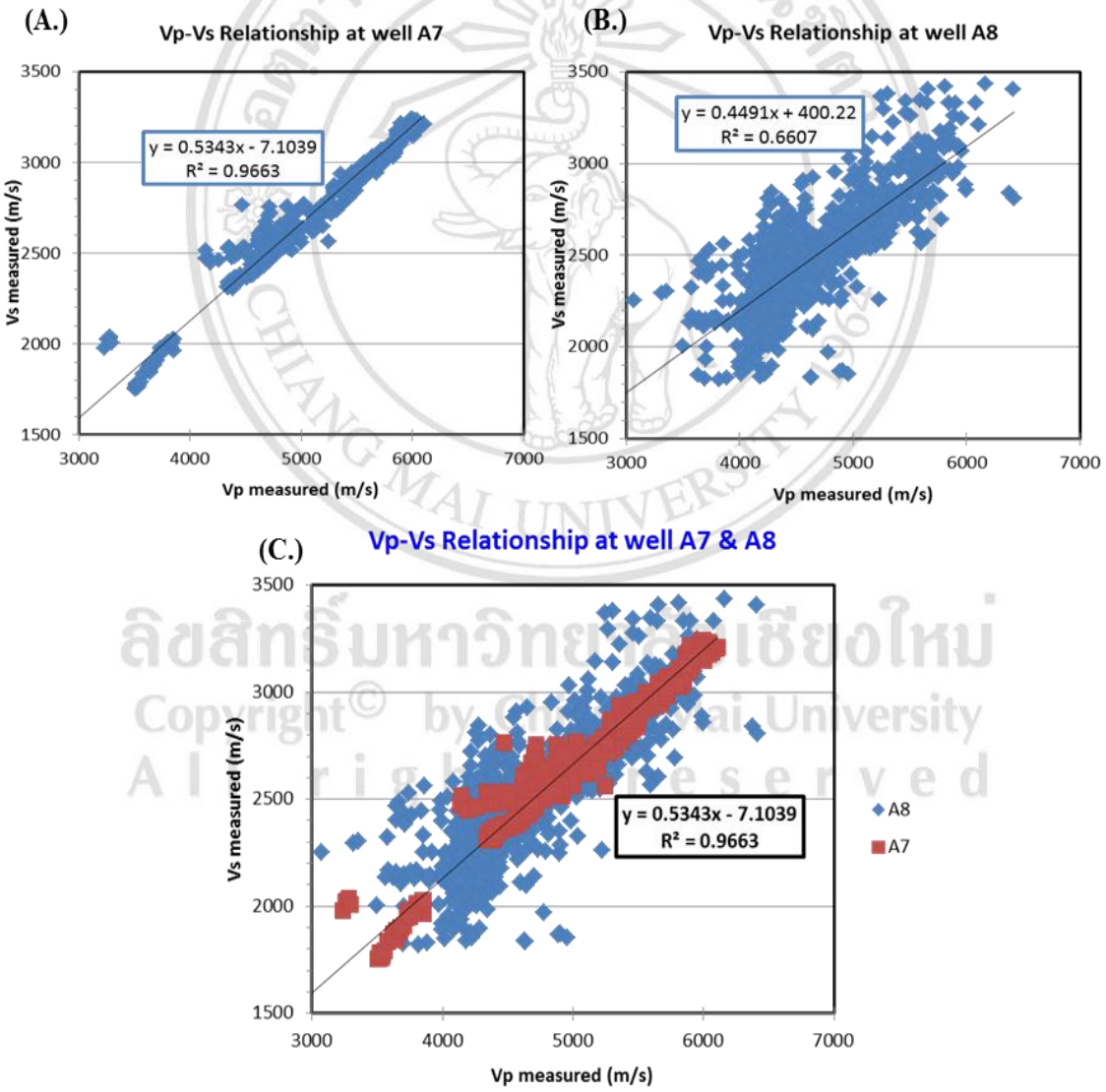

Figure 1.15. The cross correlation of Vp versus Vs belonging to the interval of Natih carbonate reservoir (Natih E) and subsequently empirical equation derived from these

correlations. (A) and (B) are from well A7 and A8 and (C) is the combination of both wells and practical well-derived equation for Vs estimation.

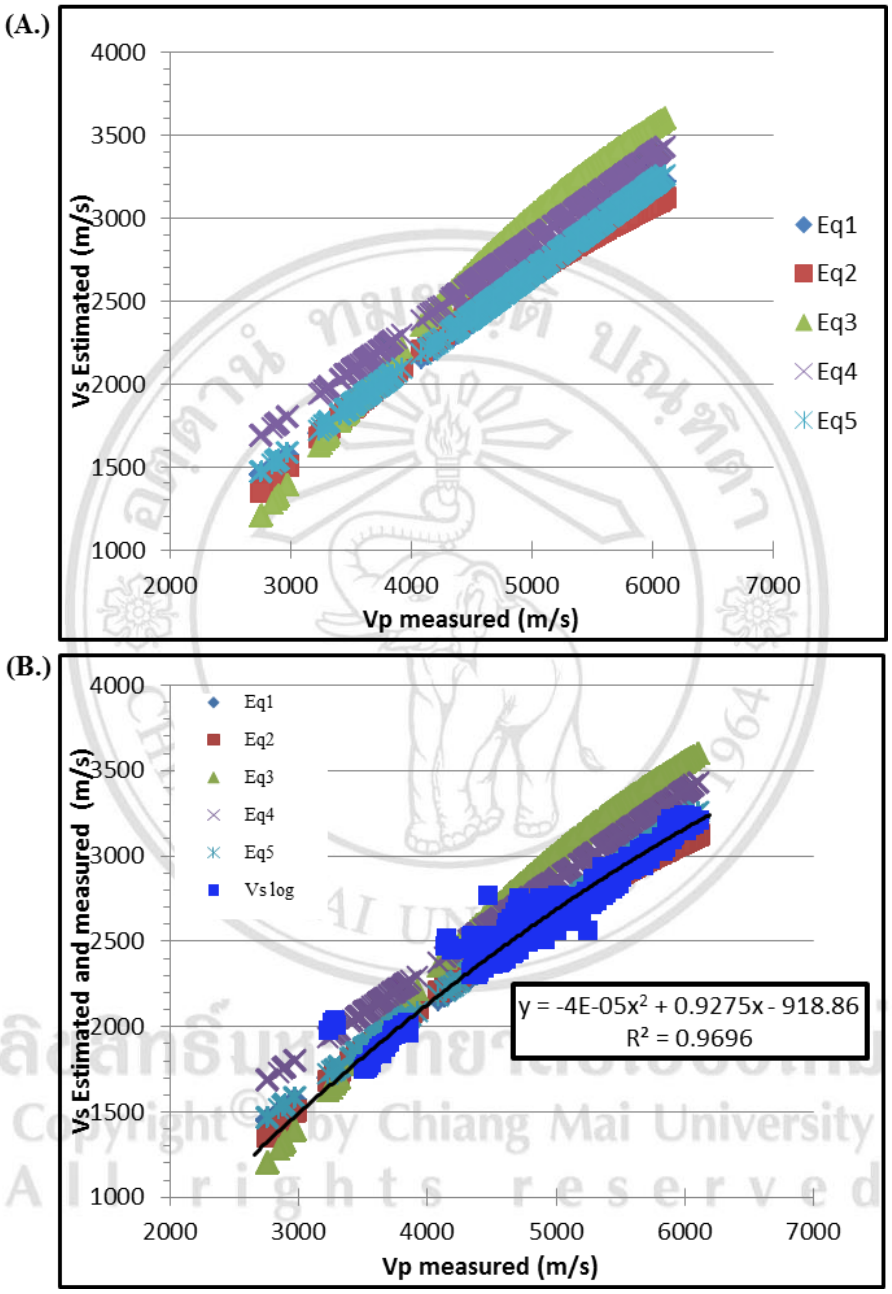

Figure 1.16. (A) The plots of estimated Vs with measured Vp from well log by using five empirical equations and (B) the previous plots added measured Vs from the same well log and derived-equation (Equation 6) for Vs estimation in this Block A.

To examine the validity of Equation 6, measured Vs from S-wave sonic logs from well A7 and A8 were compared to evaluate the degree of agreement/matching at each well (**Figure 1.17 – Figure 1.20**). Furthermore, the Greenberg-Castagna (G/C) limestone and shale (Greenberg and Castagna, 1992), and Castagna Mud rock equations (Castagna et al., 1993) of Vs estimation were also produced to compare with Vs log and Vs equation 6 (Vs_Eq6).

The variations in lithology such as limestone, limestone with thin mudstone, and thick shale interbedded with limestone had been taken into account at well A8 (depth from 2700 to 3220 m MD). **Figure 1.17** and **1.18** show the upper and lower part of well A8 respectively, there are the comparisons between Vs log and other estimated Vs logs. From those figures we can conclude that estimated Vs_Eq6 is a good fit to Vs log of well A8 except in the depth intervals of 2717 m, 2799-2803, 2814-2824, 2843, 2846, 2927-2929, 2957 m and 3203-3213 m.

From those exceptions of estimated Vs log, the conditions had been set to produce more reliable Vs log in which if the Vs log exists, Vs log would be used; if there is a gap and volume of clay (VCL) is less than or equal 0.3, then Vs_Eq6 would be used and if there is a gap and VCL is higher than 0.3, then Vs_Mud would be used (**Figure 1.19 – Figure 1.20**).

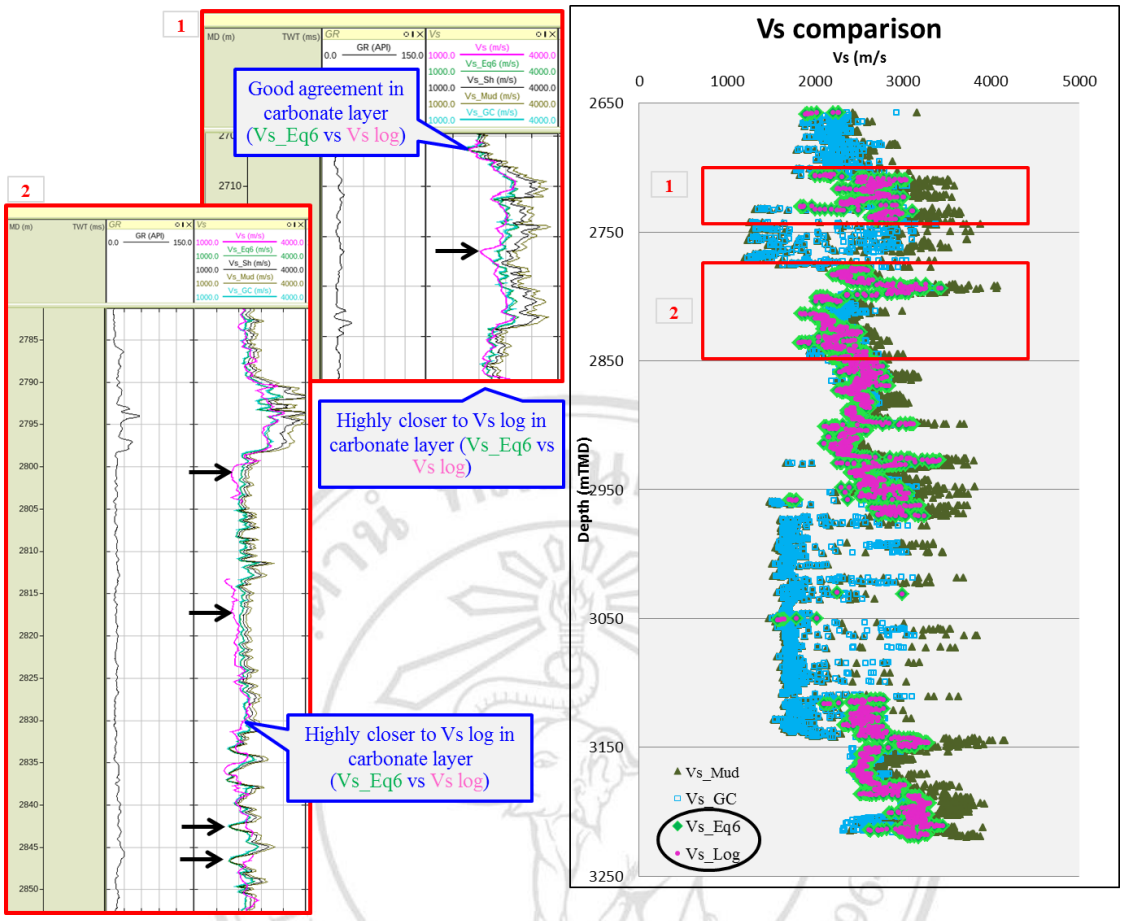

Figure 1.17. The schematic showing the Vs comparison in function of depth at well A8 which are highlighting the degree of matching between Vs log and estimated Vs_Eq6 logs. Errors in matching are pointed by black arrows.

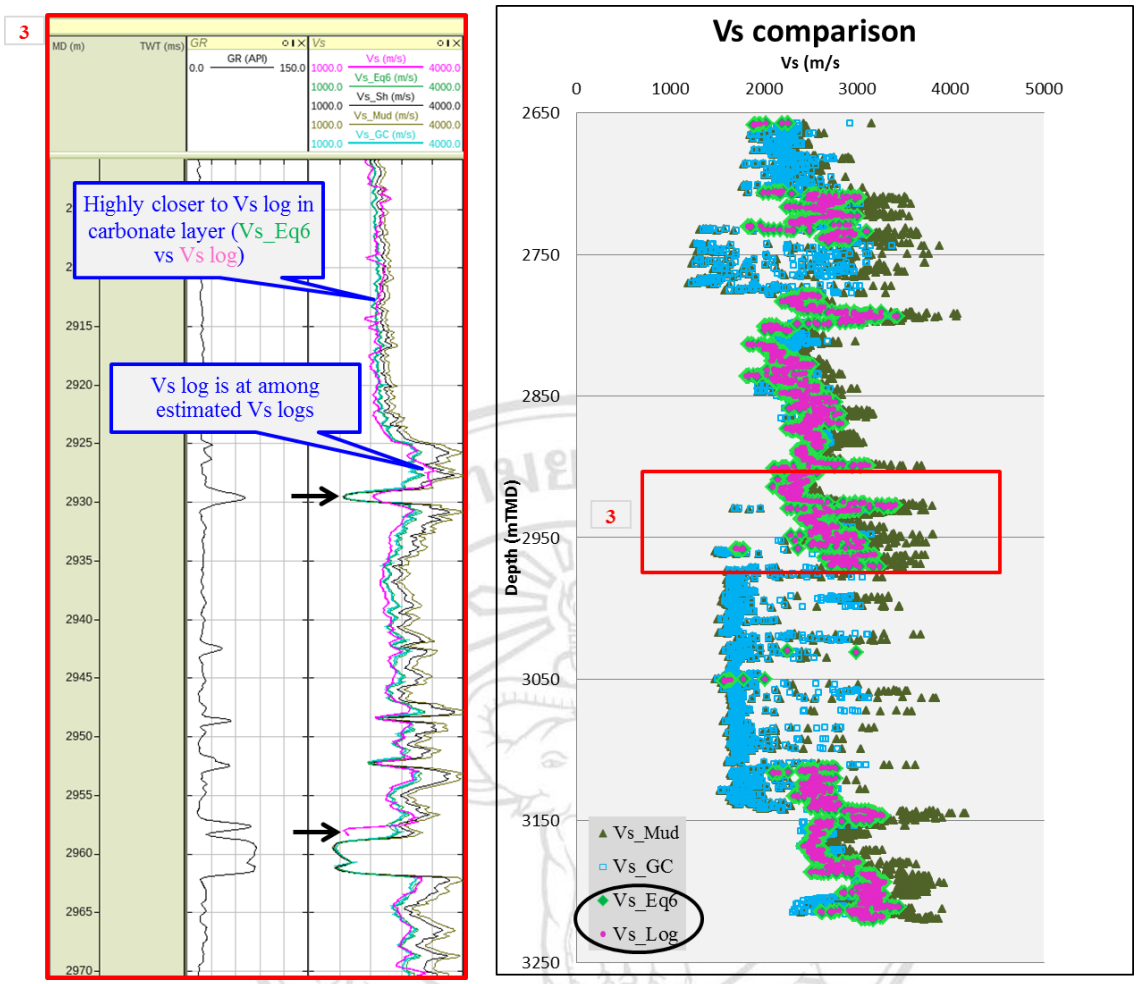

Figure 1.18. The schematic showing the Vs comparison in function of depth at well A8 which are highlighting the degree of matching between Vs log and estimated Vs_Eq6 logs. Errors in matching are pointed by black arrows.

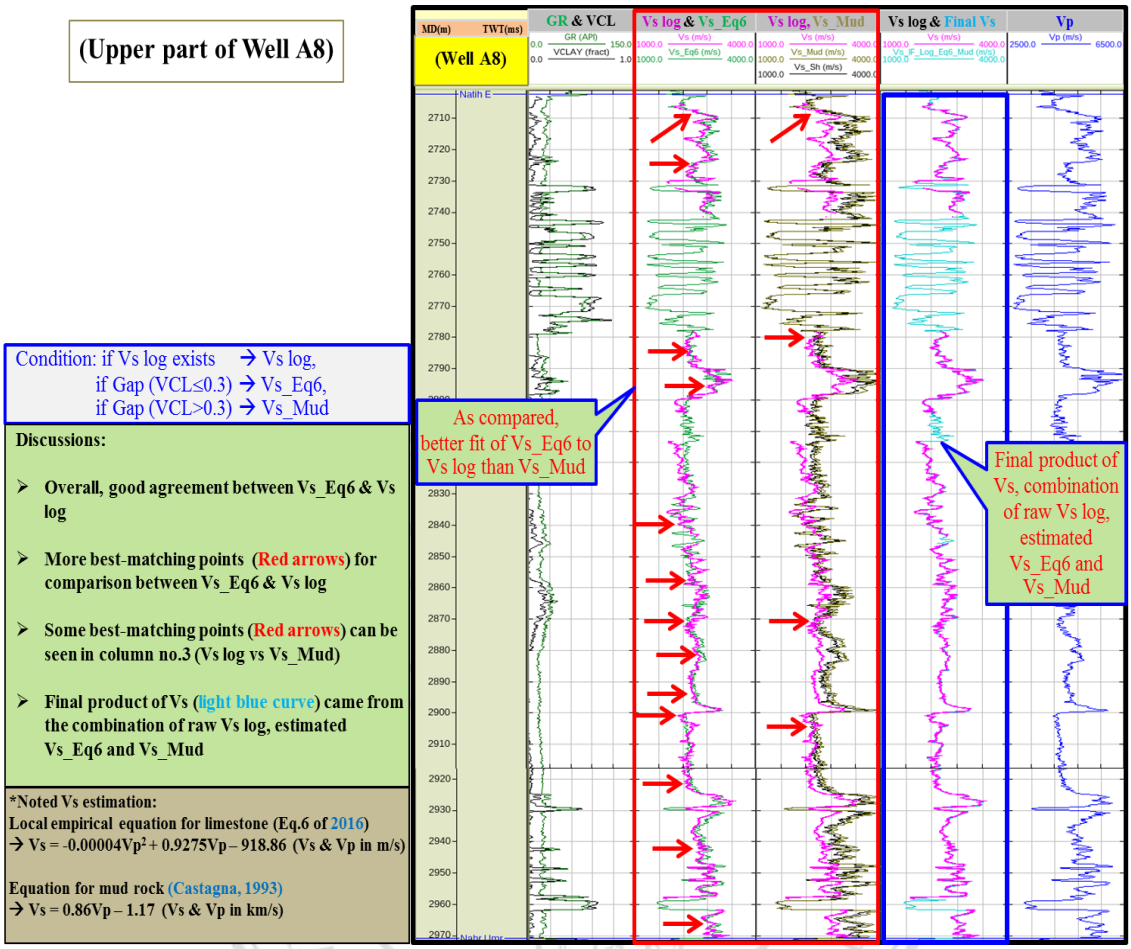

Figure 1.19. The comparisons between Vs log (pink curve) versus estimated Vs_Eq6 (green curve), Vs log versus Vs_Mud (tan curve), and Vs log versus final Vs log in column no.2-4 from left to right for the upper part of well A8.

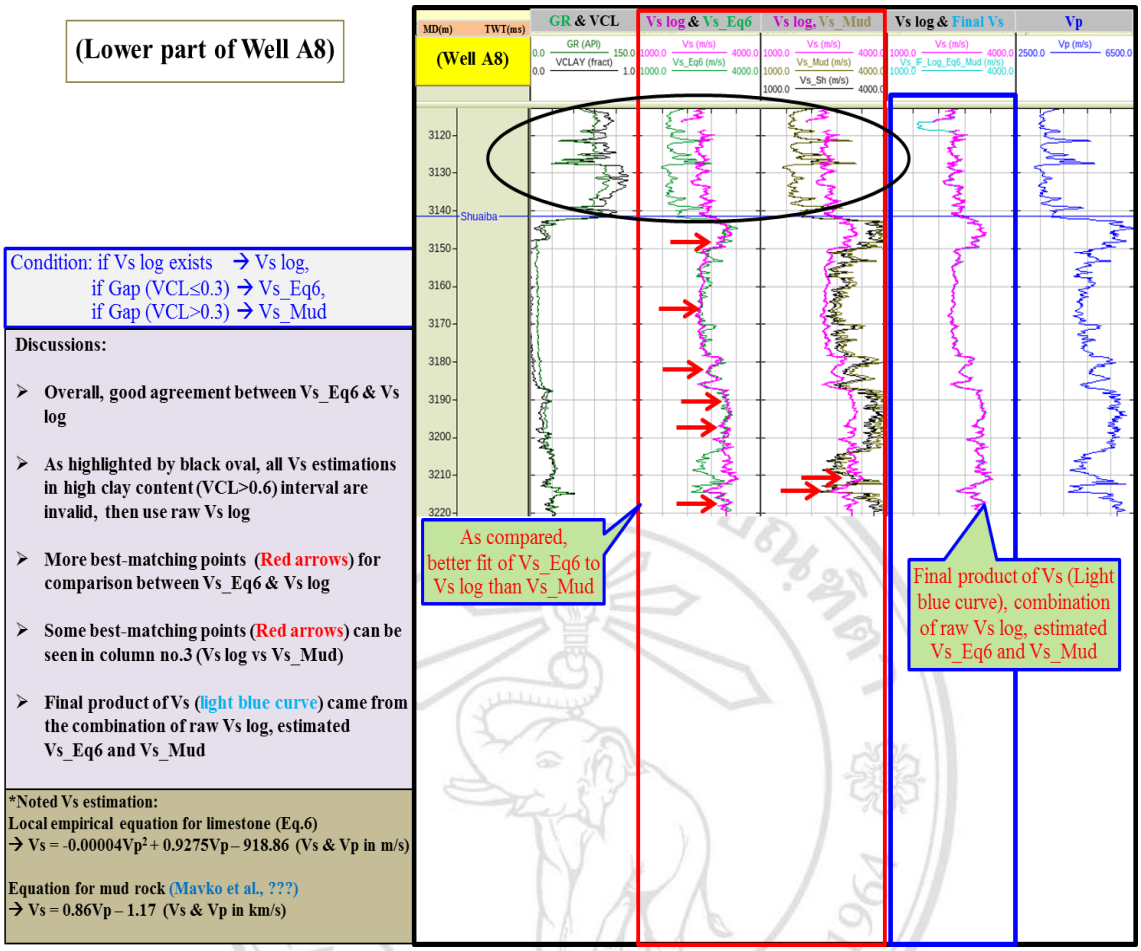

Figure 1.20. The comparisons between Vs log (pink curve) versus estimated Vs_Eq6 (green curve), Vs log versus Vs_Mud (tan curve), and Vs log versus final Vs log in column no.2-4 from left to right for the lower part of well A8.

There is small variation in lithology in well A7 where the limestone and limestone with high clay content (GR increases) are dominant (**Figure 1.21**), thus the best fit between Vs log and estimated Vs_Eq6 log can be seen. From **Figure 1.21** it can be concluded that this Equation 6 (Phaungphuak, 2016 in prep) of Vs estimation is a good predictor of S-wave velocity.

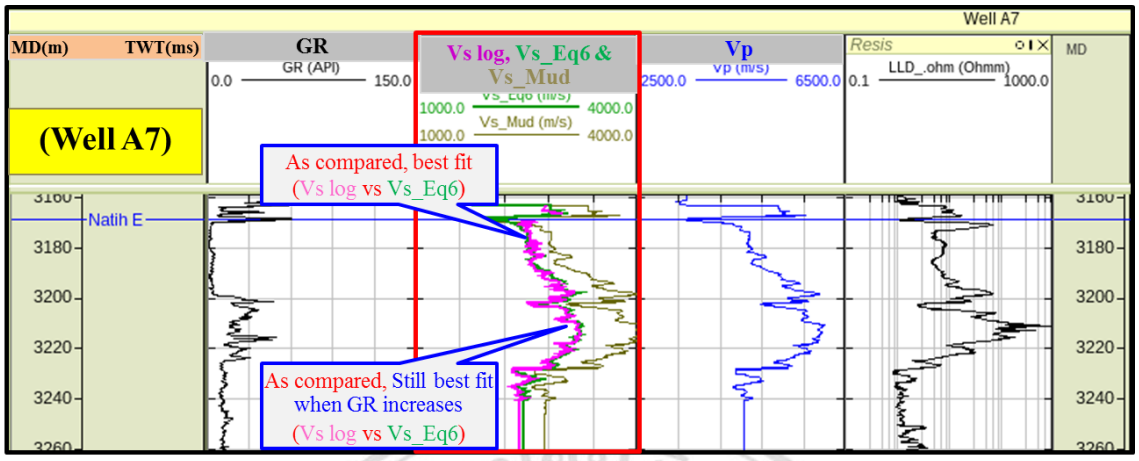

Figure 1.21. The comparisons among Vs log (pink curve), estimated Vs_Eq6 (green curve), and Vs_Mud (tan curve) for well A7. The best fit of Vs log and Vs_Eq6 log can be seen.

After all, the good agreement between Vs log and estimated Vs_Eq6 log in both well A7 and A8 makes more confidence to use this Vs estimation technique in this study. **Figure 1.22** illustrates the comparison between Vs logs and estimated Vs logs, in which the Vs_Eq6 log is final Vs data at well A7 and the combination of Vs, Vs_Eq6, and Vs_Mud logs is final Vs data at well A8. The correlation coefficient is approximately 0.97. The summary of all available well logs would be used in this study at well A8 is shown in **Figure 1.23**.

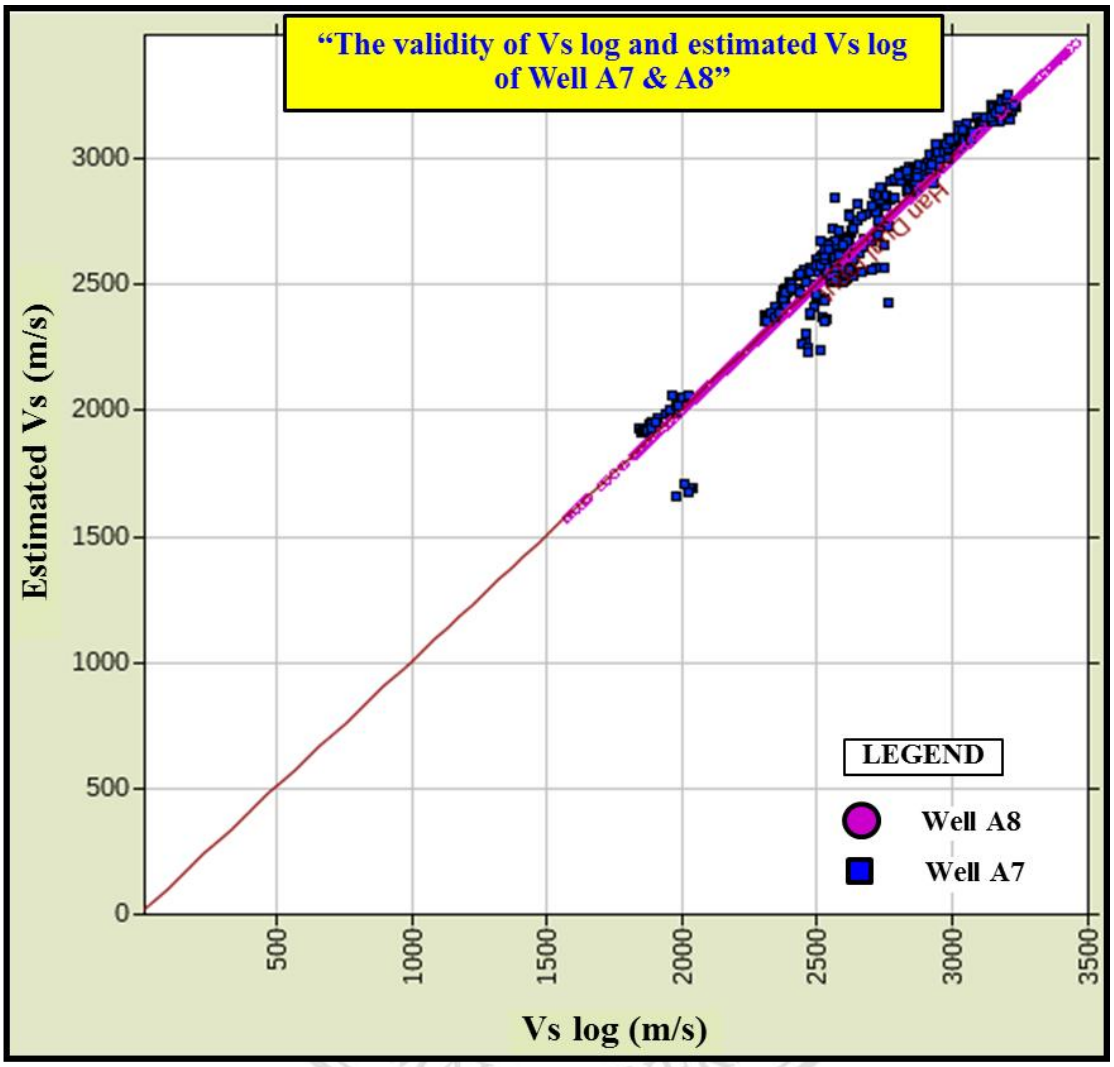

Figure 1.22. The good correlation between Vs logs and estimated Vs logs (Vs_Eq6 in well A7 and combined Vs log, Vs_Eq6 and Vs_Mud in well A8).

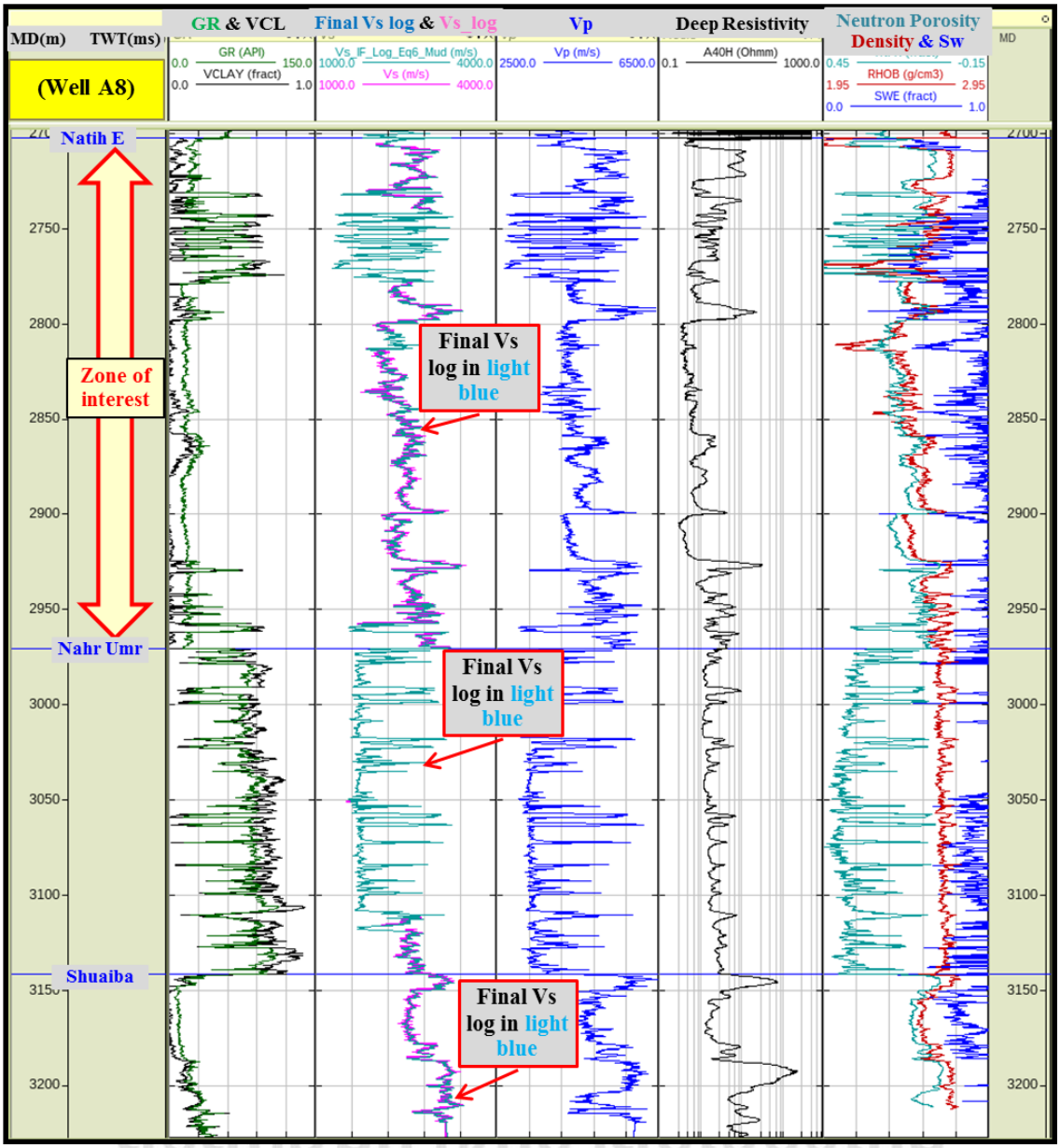

Figure 1.23. The summary of Vp, Vs, and other logs of well A8.

1.5.1.3 Other logs

The gamma ray (GR), caliper (CALI), deep resistivity (LLD), density (RHOB), and neutron porosity (NPHI) logs from all 4 wells, which exist in this study, are displayed from **Figure 1.23** to **Figure 1.26**.

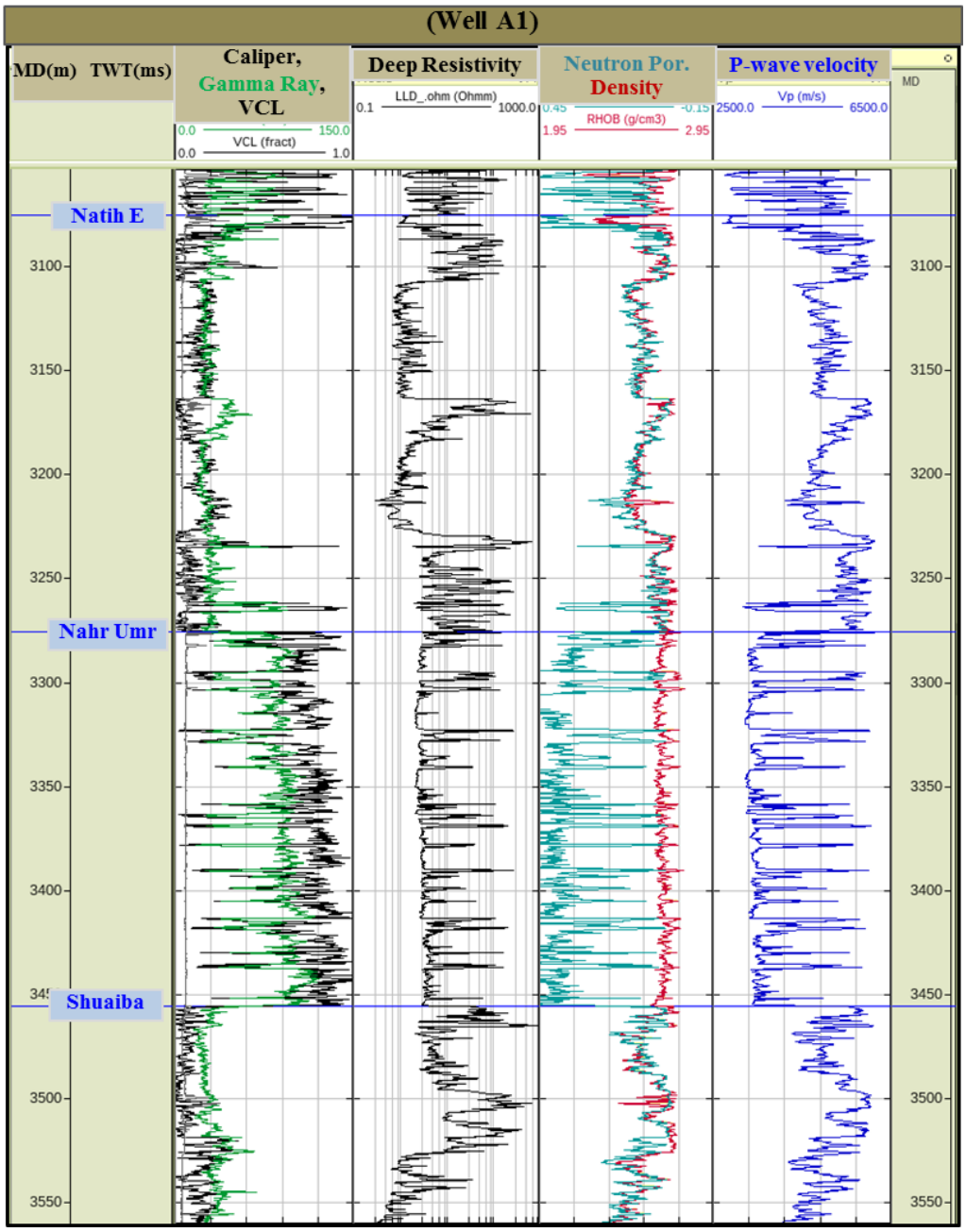

Figure 1.24. Schematic showing well logs of well A1.

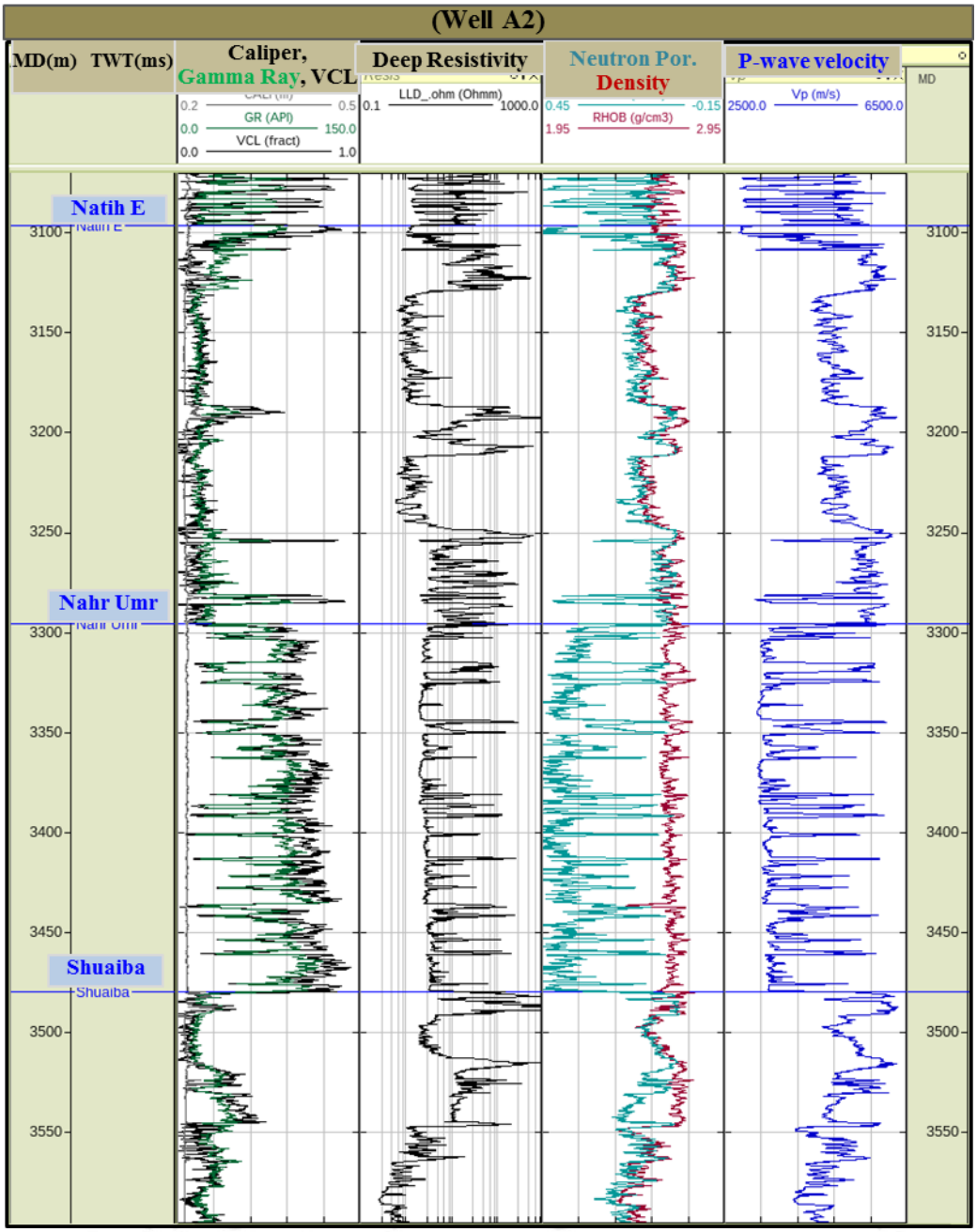

Figure 1.25. Schematic showing well logs of well A2.

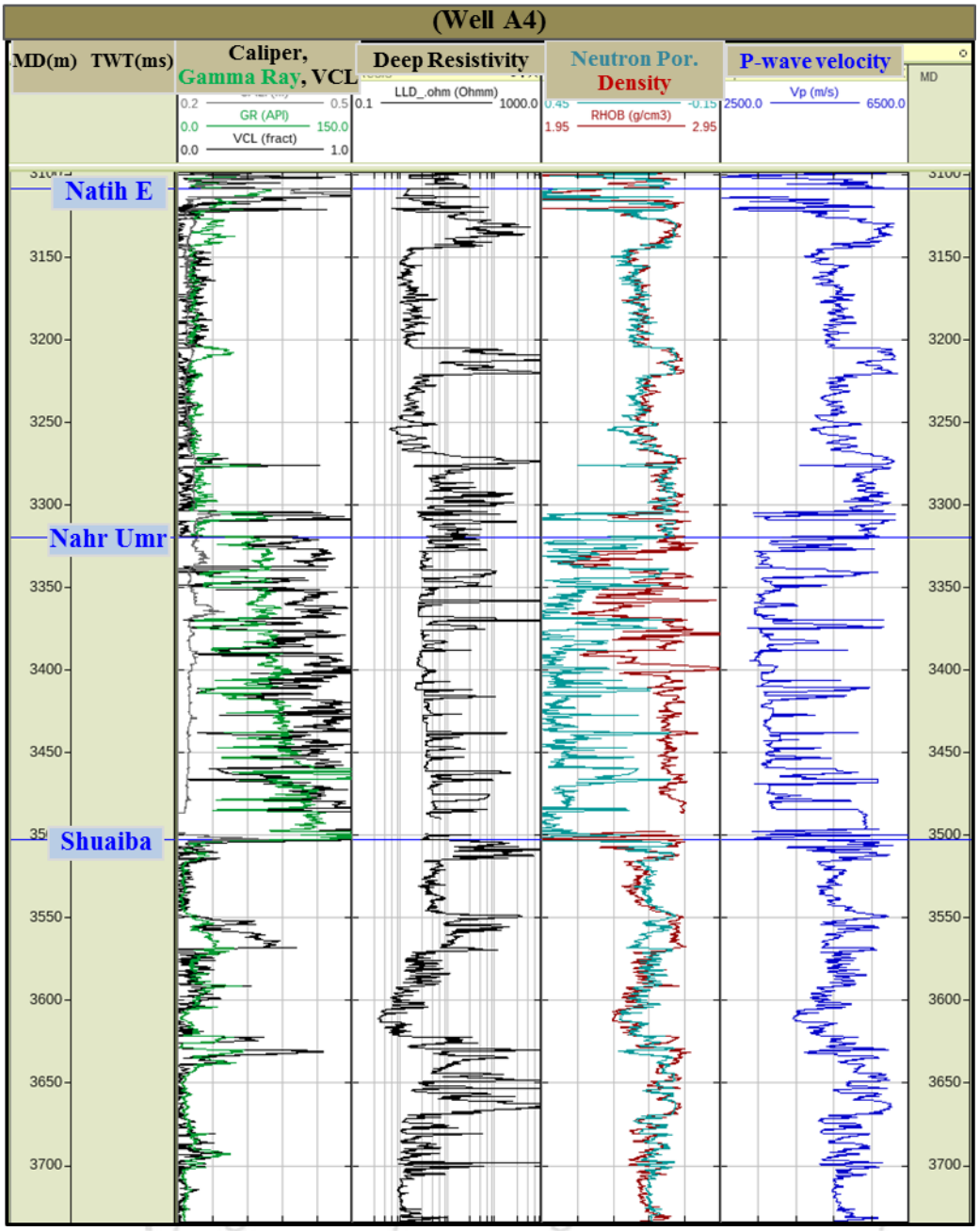

Figure 1.26. Schematic showing well logs of well A4.

From the above figure, it can be summarized that the acquired logging programs from those wells cover the formations of Natih E, Nahr Umr, and Shuaiba from top to bottom respectively. The visualizations of all measured logs (GR, CALI, VCL, LLD, RHOB, NPHI, Vp and Vs logs) look relatively acceptable. However, the rock physics modeling and interactive manipulation widgets had been used to make the process of quality control accurate and honor all data as shown in following figures (**Figure 1.27 – 1.34**).

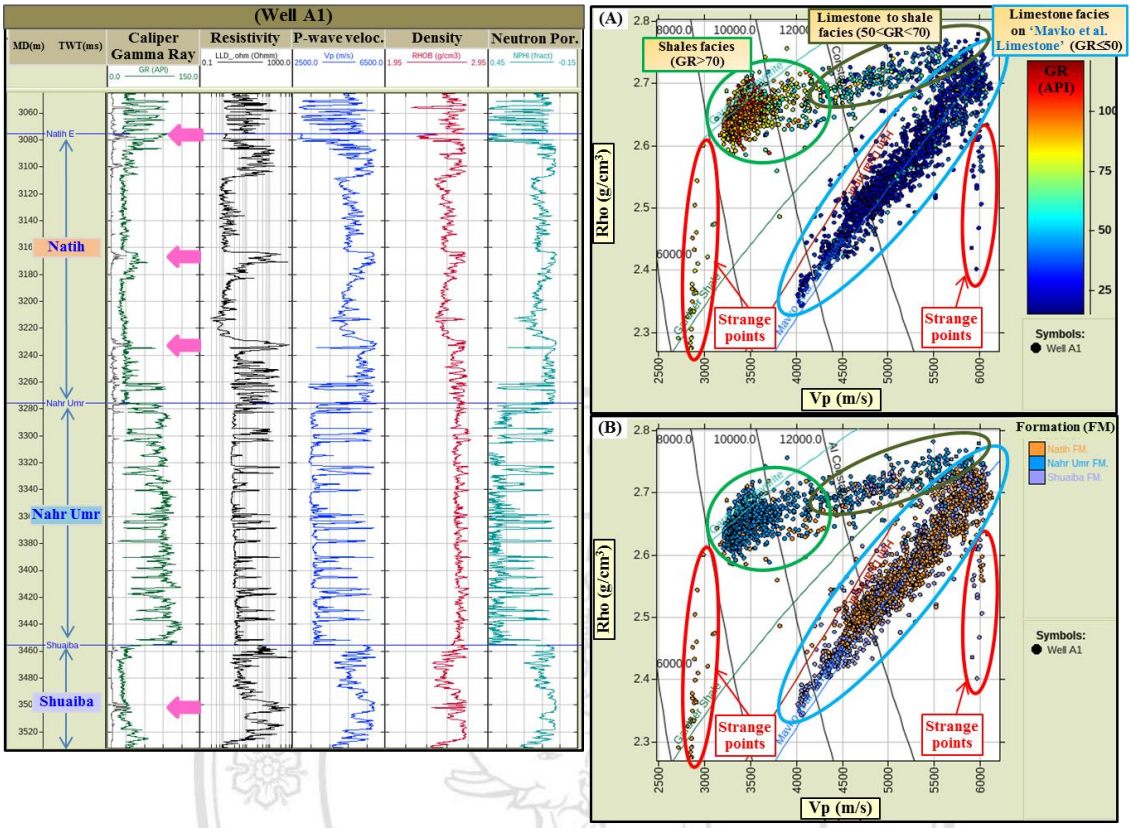

Figure 1.27. Well-log display from well A1 and its quality control analysis in the Vp-Rho domain. On the left, display of well logs and on the right, the crossplot of Vp and Rho with gamma ray (GR) values (A) and with formations (B).

In **Figure 1.27**, the detail of each log is displayed for interval of Natih to Shuaiba formation. There are several zones (Pink arrows) indicated larger hole-size (0.23-0.29 m or 9-11 in) than normal borehole operation (0.216 m or 8.5 in). They are clearly located in the intervals of formation containing more clays or shales which in fact the swelling of clay minerals normally occurred due to the use of water-based mud (WBM) during drilling. Those could be called wash out zones.

In the same figure, the crossplot between Vp and Rho shows that three facies can be identified: limestone, limestone to shale, and shale (**Figure 1.27-A**). The points of limestone facies lie totally on the Mavko et al. Limestone (1998) line which also corresponded to the gamma ray values less than or equal 50 API units. The points of other facies fall between the lines of Gardner Shale and Gardner Anhydrite (1974), and Mavko et al. Limestone (1998) at which could be interpreted as the interchange of limestone to shale (50<GR<70) or just limestone to shale facies and the shale facies for those point having GR higher than 70 API. Besides these facies, there are strange points highlighted by red ovals. To focus in another point of view, **Figure 1.27-B** illustrates the Vp – Rho domain with formations in which those strange points belonging mainly to Natih formation (orange points) and some from Shuaiba formation (violet points). To figure out this issue, point matching is performed between well log display and crossplot as shown in **Figure 1.28**.

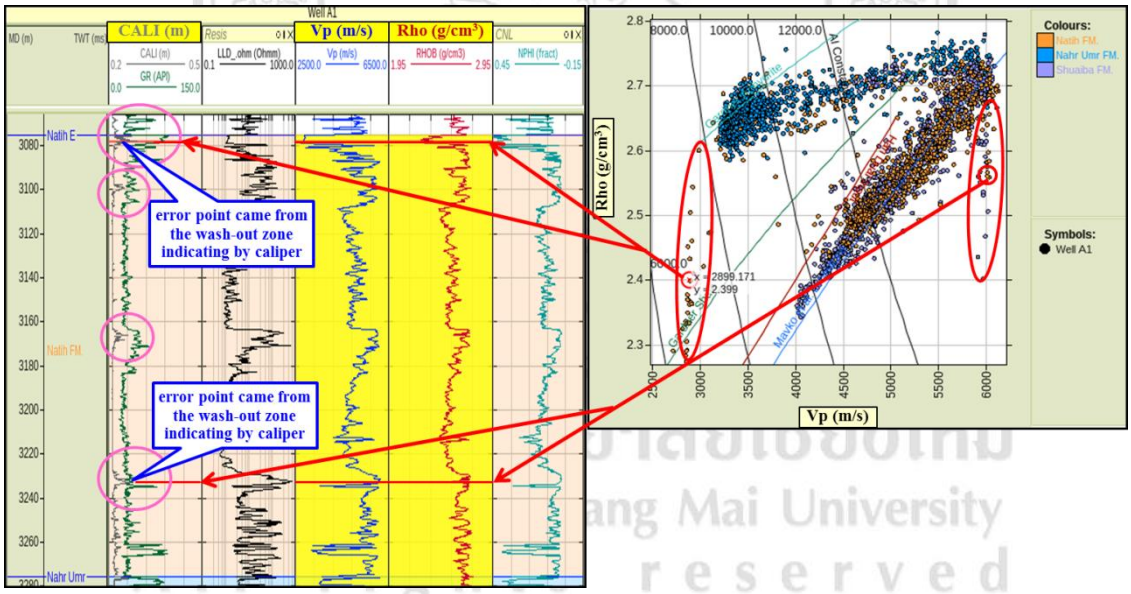

Figure 1.28. Schematic showing quality control analysis in Vp and Rho domain highlighting individual strange points that corresponded to wash-out zones (Pink circle).

Those strange points are corresponding to the identified-washout zones (pink circle) or the zone of large hole-size expressed by caliper log. It means that the incorrect Vp and Rho values affecting by wash-out problem; hence the log conditioning in specific depth interval is necessary. Accordingly, the log editing is carefully done based on relative rock properties and in situ characteristics. The real time point matching with polygon has also been considered during log-editing job for Vp and Rho logs.

In **Figure 1.29**, two cross-plots of Vp and Rho and well-log display comparing before and after log conditioning in well A1 are depicted. The quality control and data conditioning of well A2, A4 and A8, using similar techniques, can be seen in **Figure 1.30-1.32**.

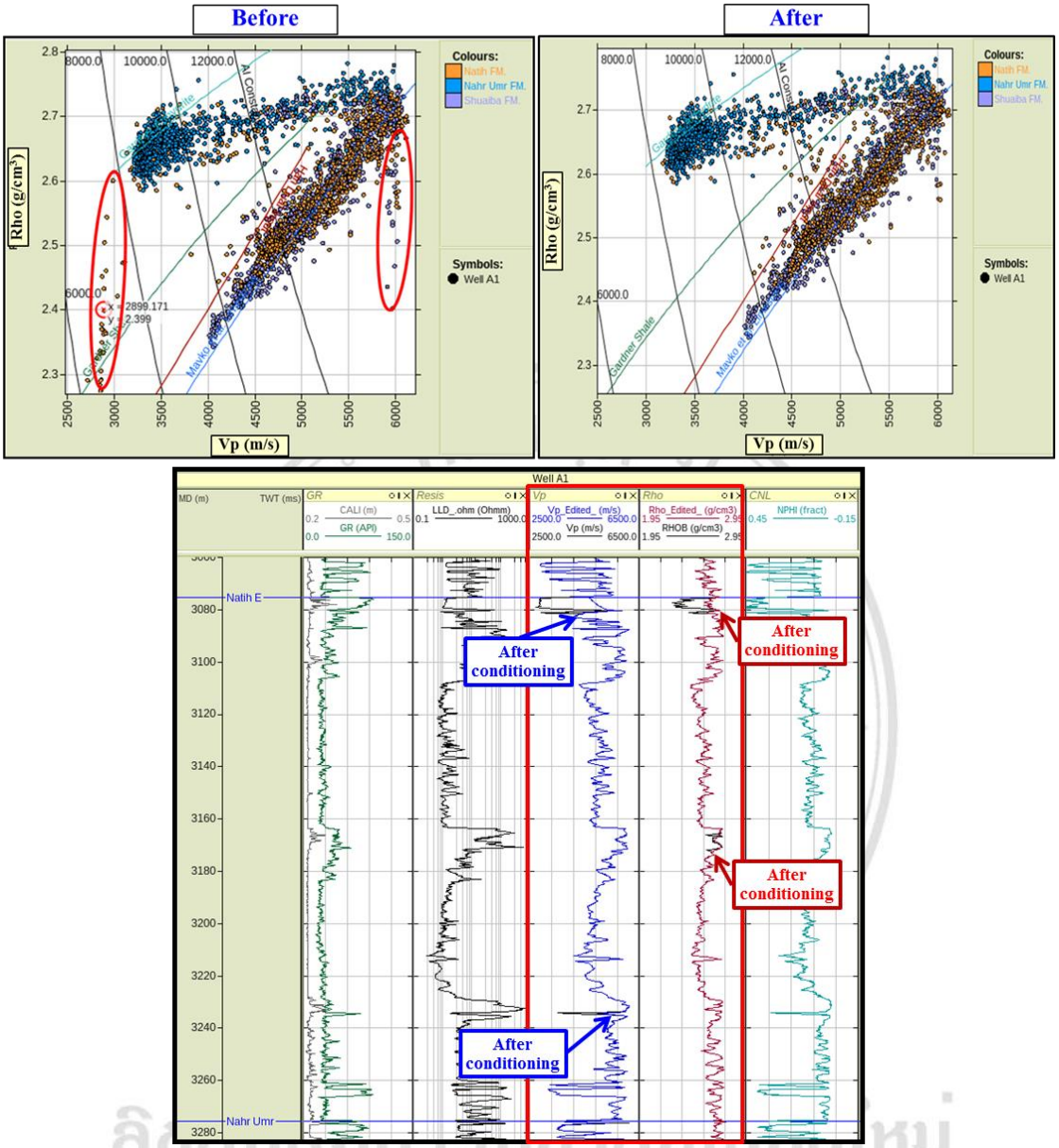

Figure 1.29. The crossplots (Top) and well-log display (Bottom) of Vp and Rho showing before and after log conditioning (editing of points in wash-out zones) at well A1.

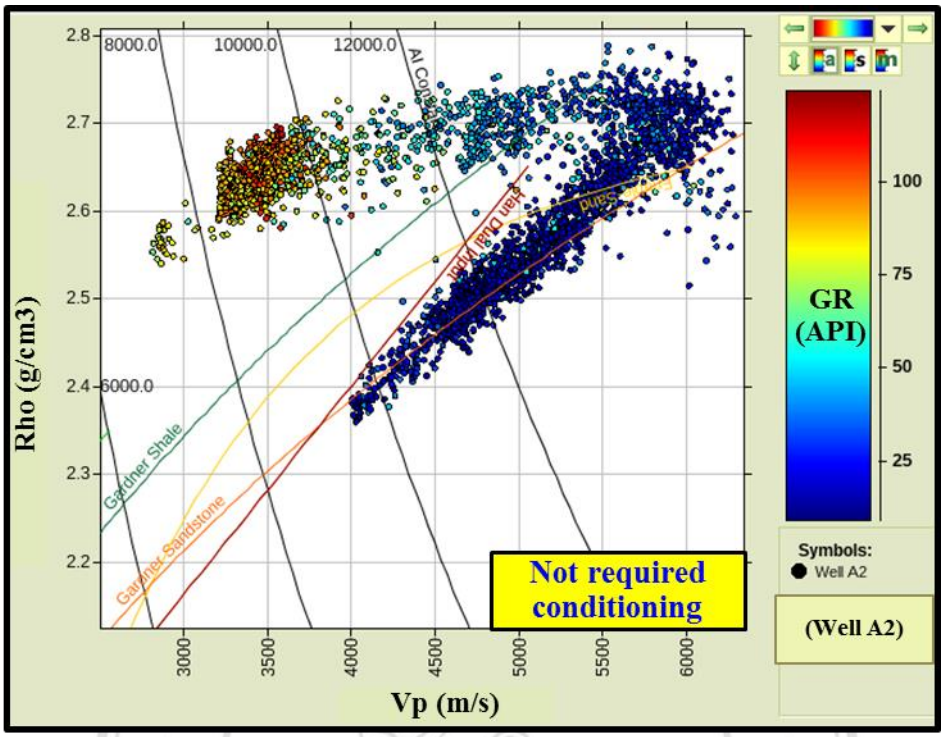

Figure 1.30. The crossplots of Vp versus Rho showing no conditioning at well A2.

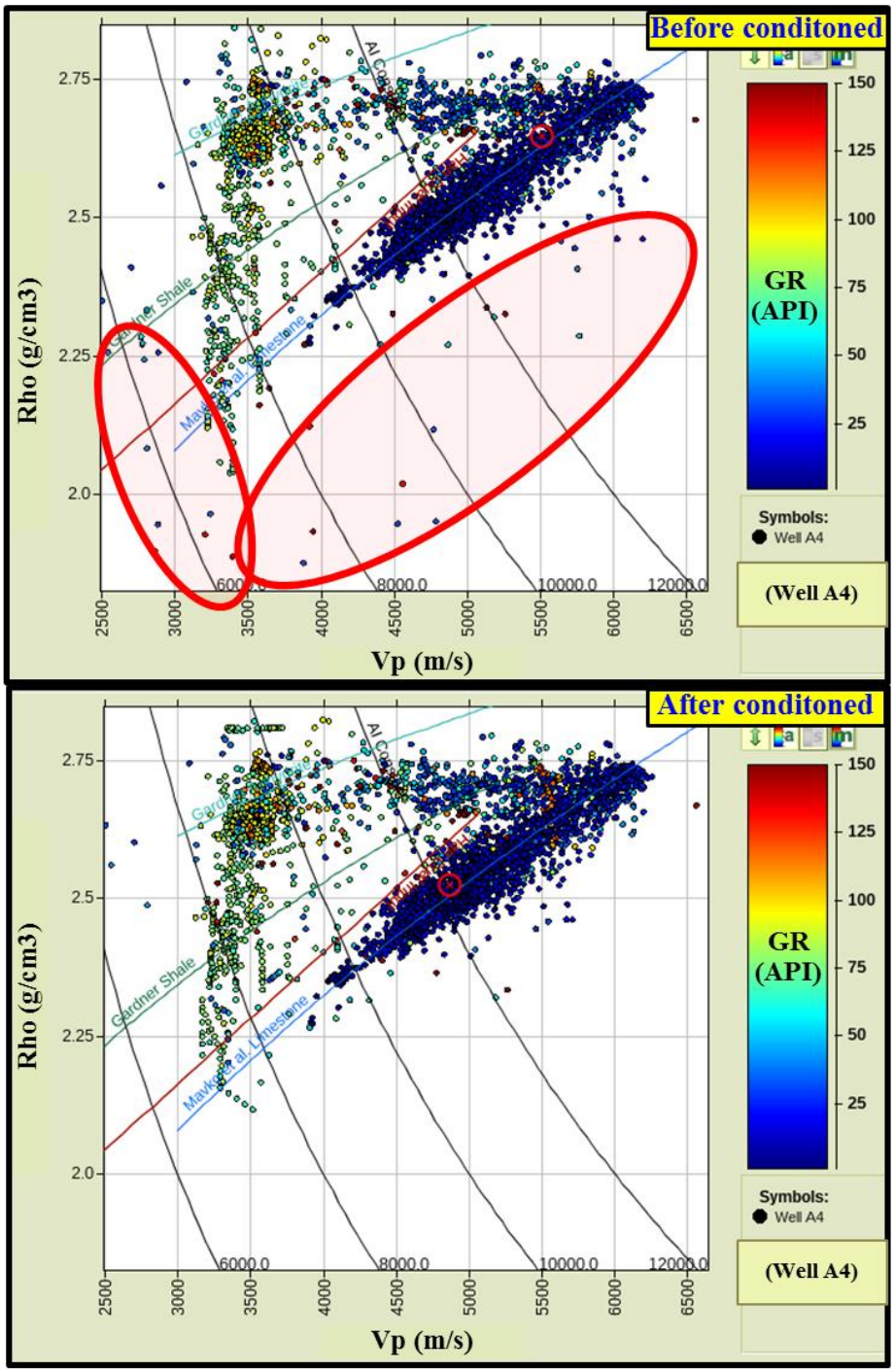

Figure 1.31. The crossplots of Vp versus Rho showing before and after conditioning at well A4.

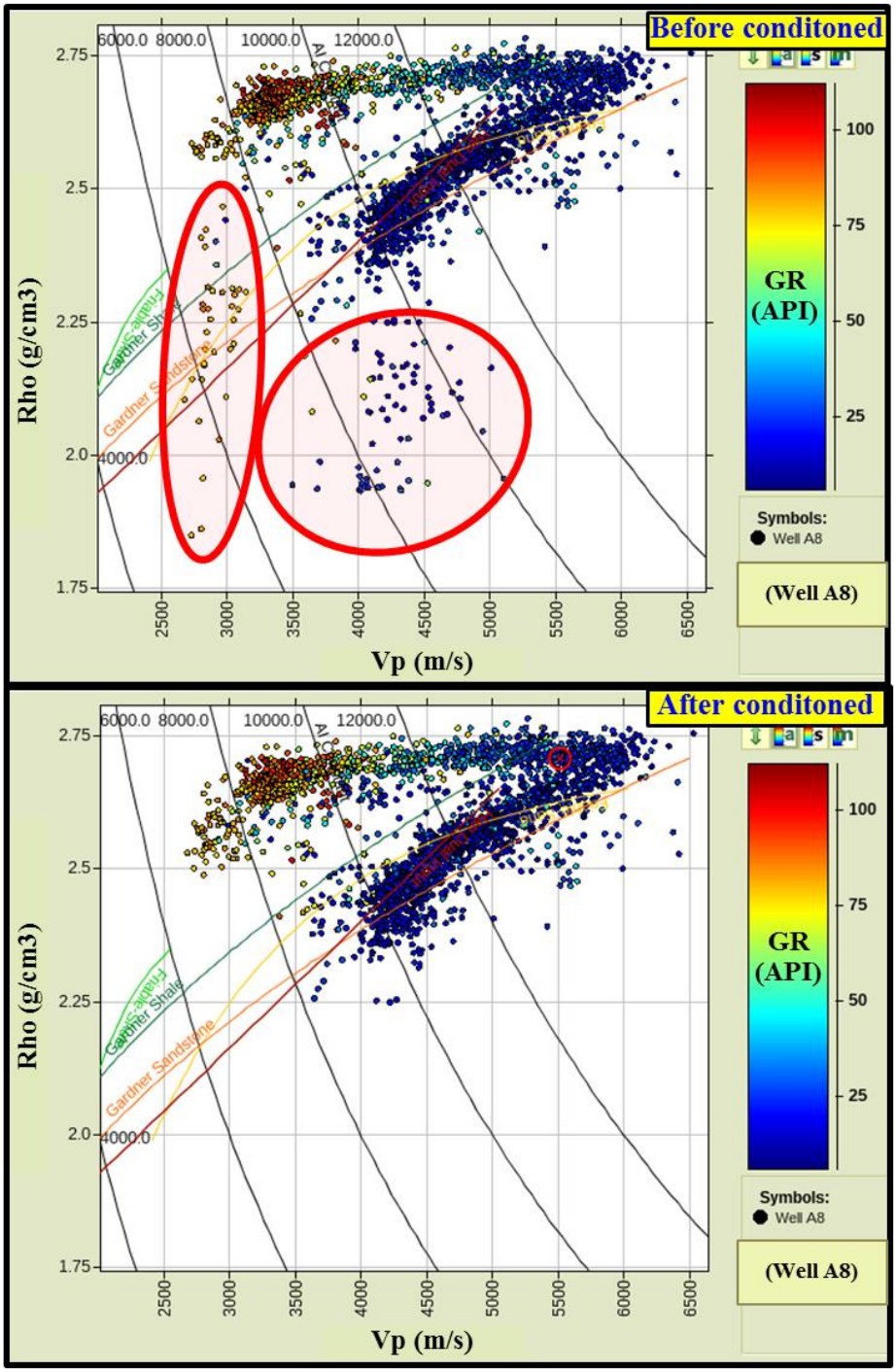

Figure 1.32. The crossplots of Vp versus Rho showing before and after conditioning at well A8.

Next, the data checking for velocity-porosity, density-porosity, and resistivity-gamma ray relations are performed by cross-plotting them (**Figure 1.33-1.34**). In the plot of P-wave velocity versus neutron porosity (Vp-vs-NPHI), there is wide range of porosity values from all rocks in which the bound of velocity-porosity relations could be established (orange line). It represents the strong relationship between velocity and porosity indicating the velocity decreases with porosity increase (**Figure 1.33-A1**). From Han's work (1986), it suggests that the increase of clay content (poorer sorting) decreases the porosity. **Figure 1.33-A2** illustrates the identified group of carbonate reservoir using clay volume (Vcl) cut-off less than 0.3. This identified group contains 4,000-6,100 m/s of P-wave velocity (Vp) and 0.03-0.25 of neutron porosity (Por). The use of clay volume clearly improves reservoir identification.

Lastly, the plots of density versus neutron porosity (Rho vs NPHI) and resistivity versus gamma ray (LLD vs GR) in **Figure 1.34** show that the good relations among them could establish and easily identify the facies groups (i.e. limestone, limestone to shale, and shale). The density versus porosity diagram depicts the linear regressions for limestone and shales respectively (**Figure 1.34-A**) which indicate good discrimination in principle between rock types (limestone and shale). The linear equations for each rock type can be expressed as:

Log(Rho) = (-0.2515)*NPHI (for limestone) and Log(Rho) = (-0.0185)*NPHI (for shale).

In **Figure 1.34-B**, the similar identified facies could be seen in the plot of resistivity versus gamma ray and again the strange points lie separately from others, so we are able to highlight them (red oval). From this plot, it can be stated that each rock (facies) acts differently in the aspect of conductivity (reciprocal of resistivity).

These methodologies are also intensely applied and iterated in other wells so that spurious values can be eliminated before petrophysical and rock physics analysis.

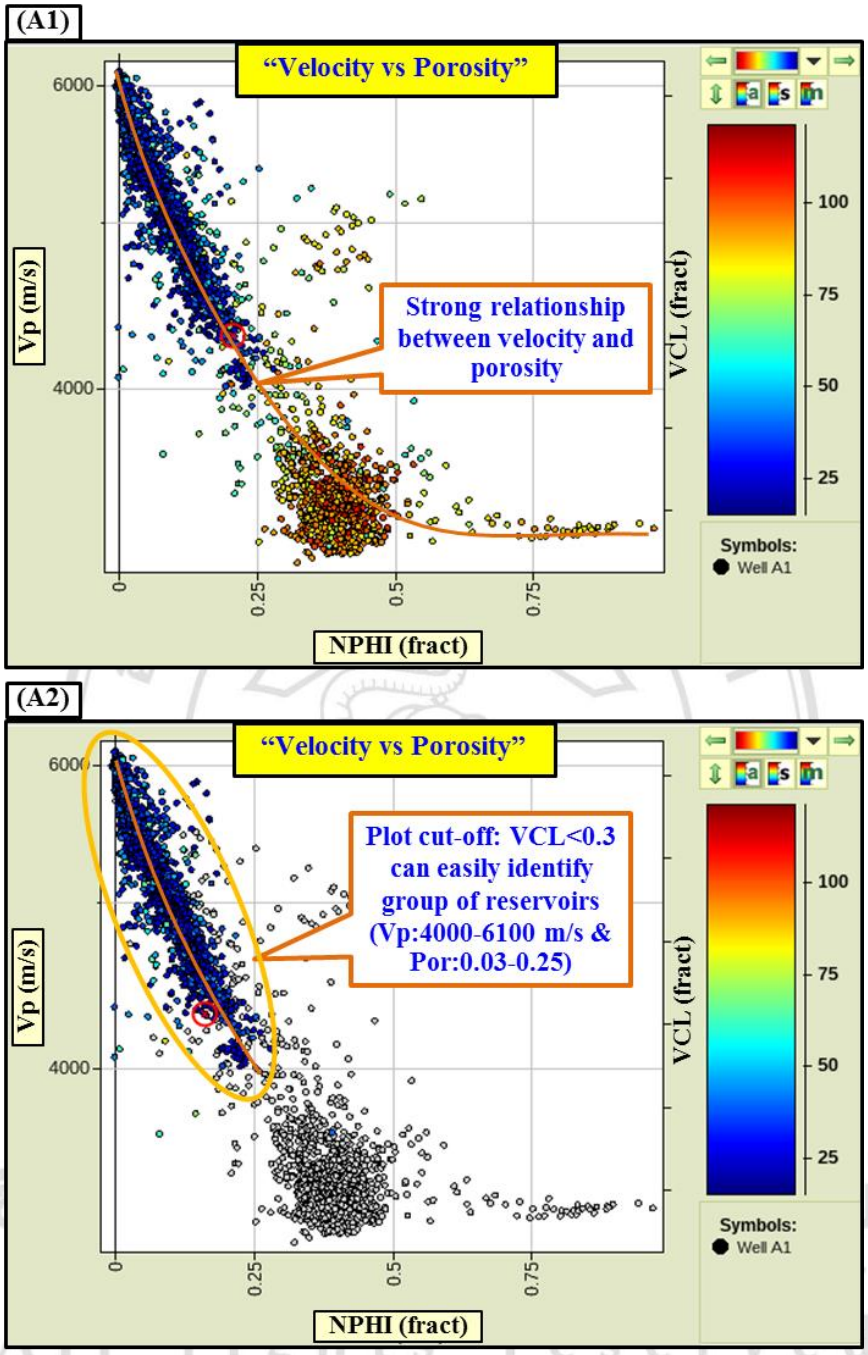

Figure 1.33. P-wave velocity (Vp) versus neutron porosity (NPHI) showing the typical bound of velocity-porosity relations and identified reservoir group.

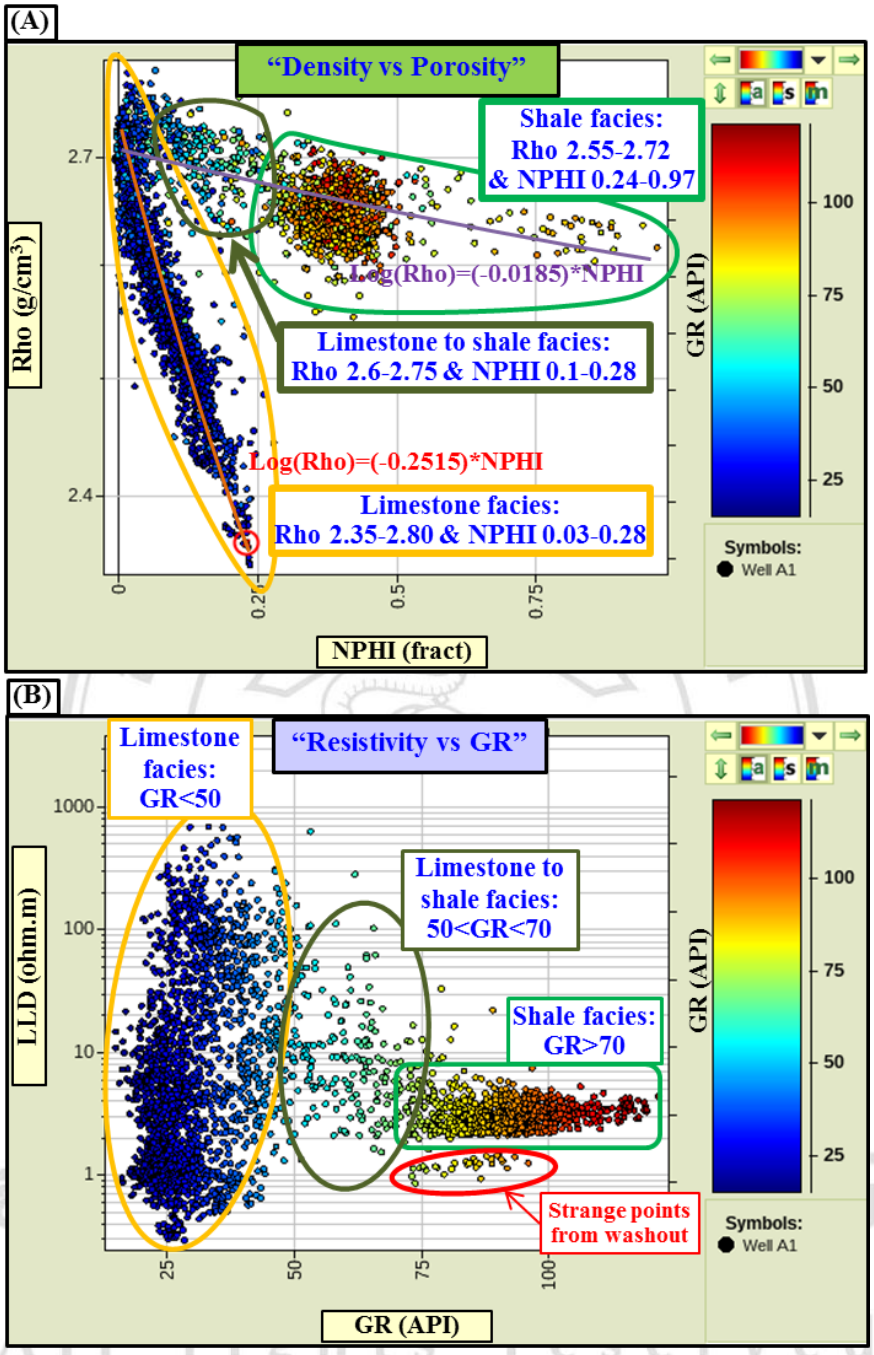

Figure 1.34. Schematic showing crossplot of Density (Rho) versus neutron porosity (NPHI) and resistivity (LLD) versus gamma ray (GR), representing facies group and individual properties.

1.5.2 Quality control of seismic data

The quality of 3D seismic data is good (**Figure 1.35**) and we are able to recognize the strong reflectors at around 1700 – 2100 ms two way time (TWT), corresponding to the very high acoustic impedance contrast at the top of carbonates (Natih and Shuaiba formations).

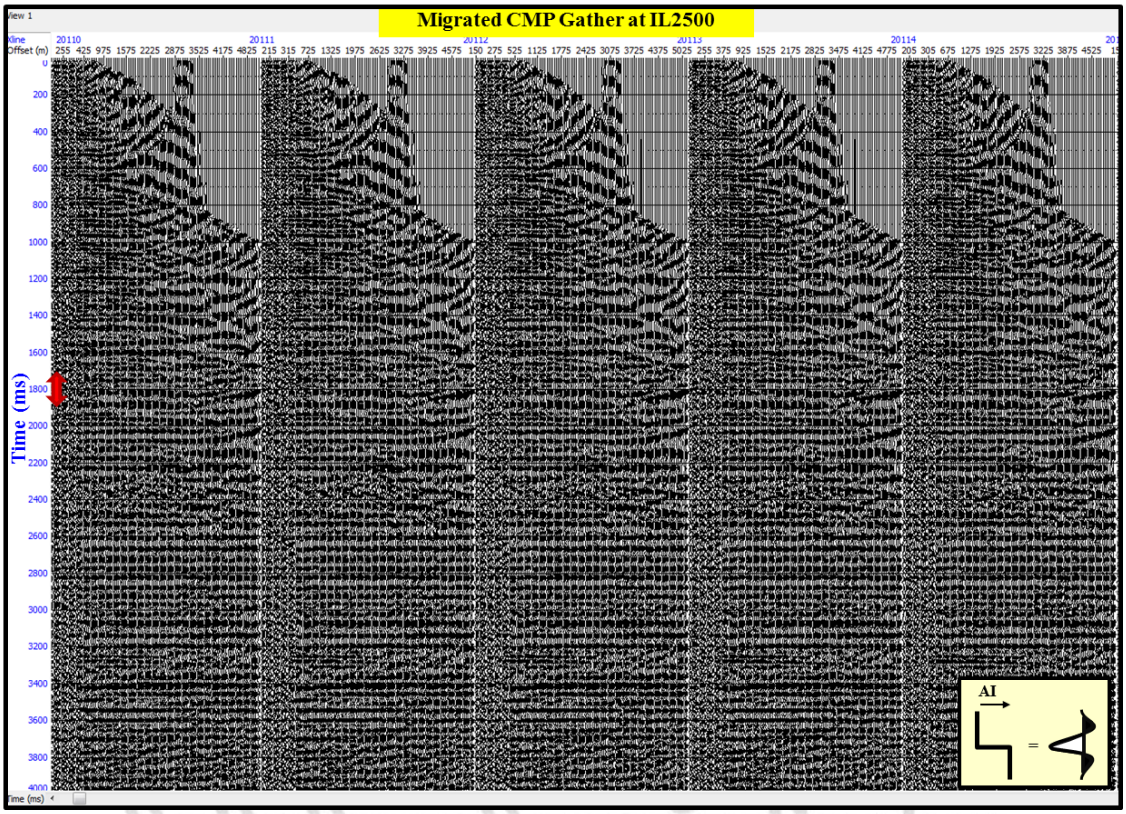

Figure 1.35. Five PSTM-migrated CMP gathers from inline (IL) 2500 with crosslines 20110-20114. The zone of interest is highlighting by red arrows which are around 1700-2100 ms TWT. [The arrows look more like 1700-1900 ms. Thanks for the cartoon of the polarity convention!]

The 2013 reprocessing was performed to these common midpoint (CMP) gathers, but the noise and other residual unwanted signals still remained in the seismic data. However, the study is not intended as a comprehensive seismic processing effort, but rather aims to condition the gathers as appropriately as possible to improve the quality of amplitude variation with offset (AVO) and inversion results. The seismic conditioning such as outer mute function was applied on those gathers as Singleton

(2009) revealed the advantages and necessary of performing some conditioning prior to pre-stack impedance inversion.

The considerations of data quality including signal-to-noise ratio (SNR) with gather alignment, and amplitude scaling involving true amplitude recovery and scaling with offset would be generally done as suggested by many authors (e.g. Singletone, 2009; Simm and Bacon, 2014).

The comparison between raw and conditioned seismic CMP gathers at inline 2500 after stretch muting **(Figure 1.36)** shows significant improvement in exhibition and reflector recognition. Super gathering has been performed to increase signal-to-noise. The great improvement can be clearly seen in **Figure 1.36** to **Figure 1.37** at which the comparison between raw and conditioned seismic gathers with highlighted zones is depicted. In **Figure 1.38**, there is super gather at inline 2500 and crossline 20110-20114 displaying the range of incidence angle of this data set by using P-wave sonic log of well A8, corrected for the well-tie time:depth function, as the velocity function.

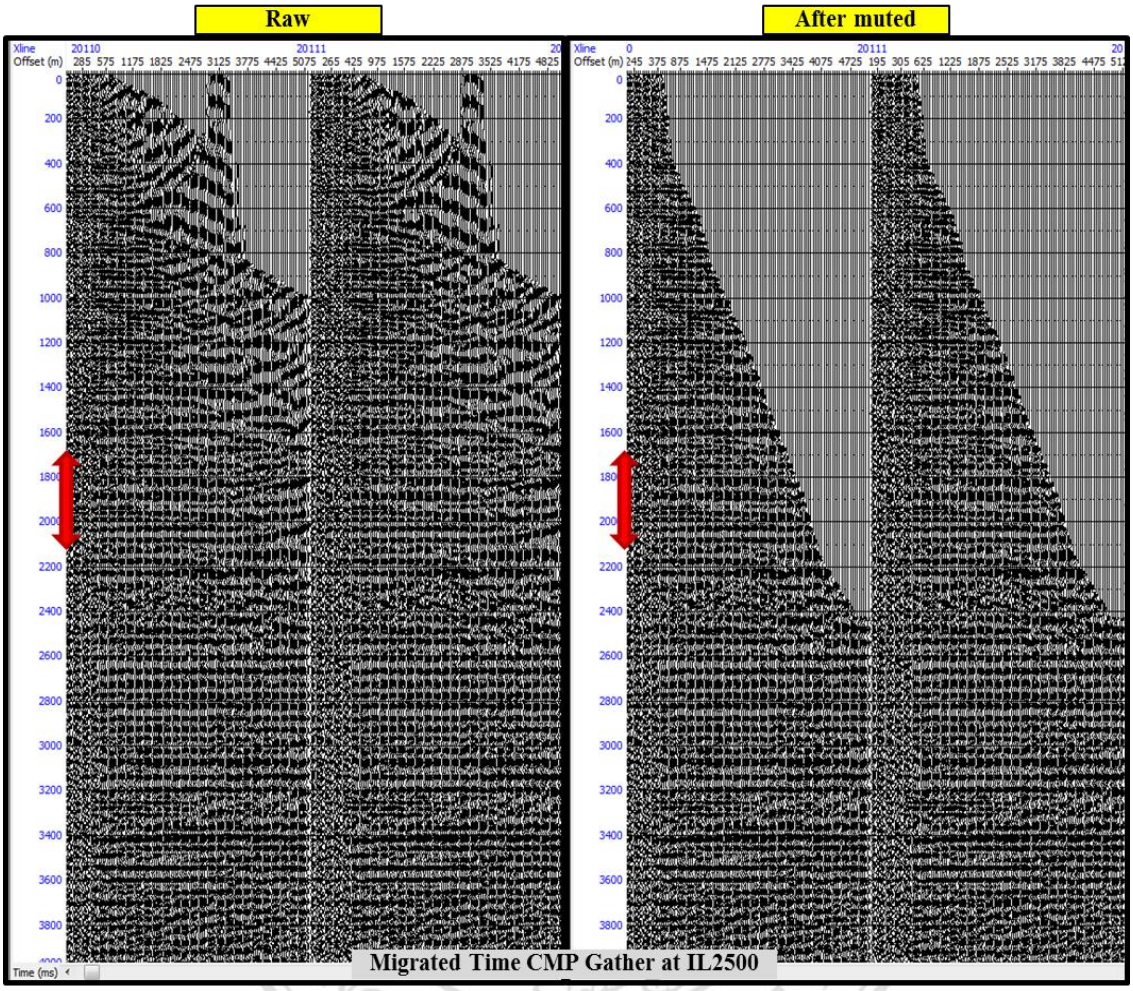

Figure 1.36. Raw (left) and muted (right) gathers at inline 2500 and crossline 20110-20111. Zone of interest is highlighted by red arrow. Horizontal axis is offset (m) and vertical axis is time (ms).

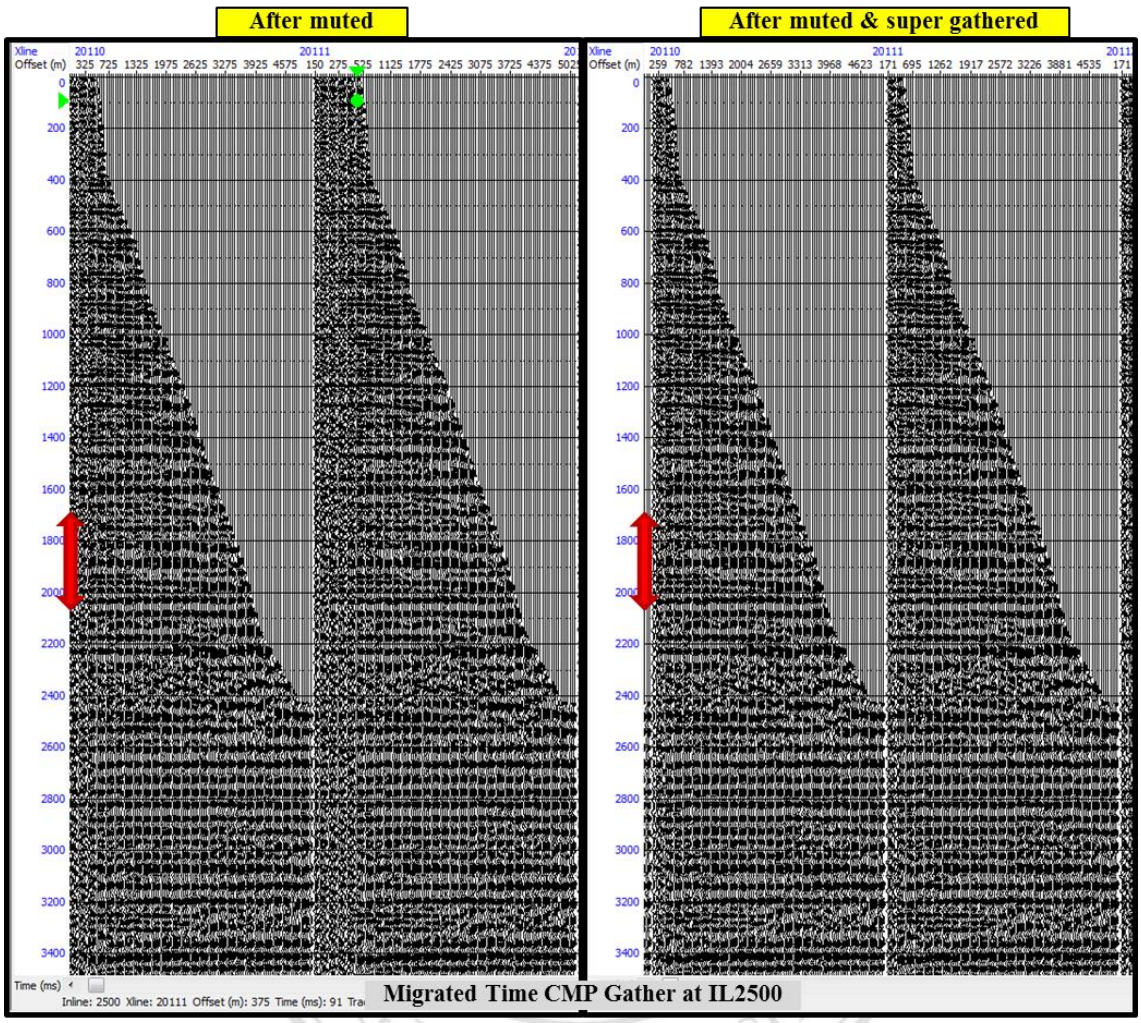

Figure 1.37. Muted (left) and super (right) gathers at inline 2500 and crossline 20110-20111. Zone of interest is highlighted by red arrow. Horizontal axis is offset (m) and vertical axis is time (ms).

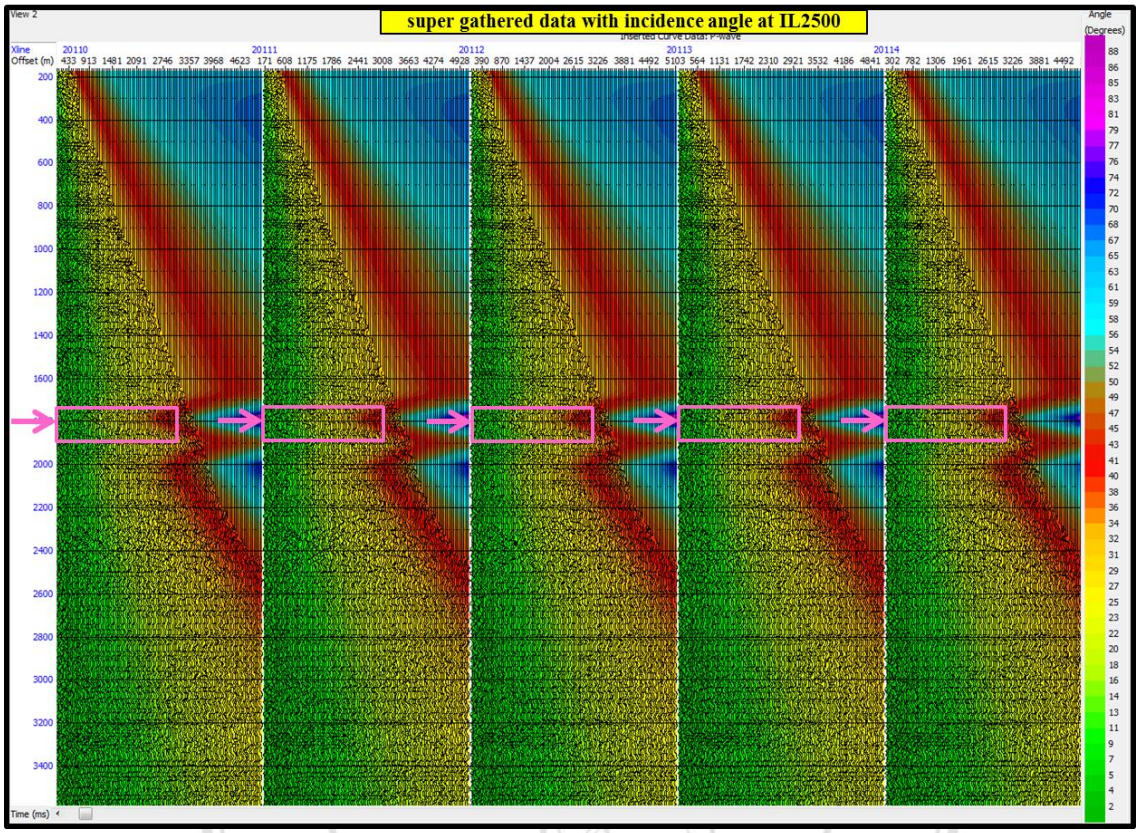

Figure 1.38. Super gather at inline 2500 displaying the range of incidence angle which used the corrected P-wave velocity of well A8 as velocity function. Top of target is about 1800 ms TWT. Horizontal axis is offset (m) and vertical axis is time (ms TWT).